Ocean Sci., 22, 791–820, 2026
https://doi.org/10.5194/os-22-791-2026

Ocean Science Open Access EGU

Iron isotope insights into equatorial Pacific biogeochemistry

Capucine Camin[1], Marie Labatut[1], Catherine Pradoux[1], James W. Murray[2], and François Lacan[1]

[1]Université de Toulouse, LEGOS (CNES/CNRS/IRD/UT), Toulouse, France
[2]School of Oceanography, University of Washington, Seattle, Washington, USA

Correspondence: Capucine Camin (capucine.camin@orange.fr) and François Lacan (francois.lacan@cnrs.fr)

Received: 15 September 2025 – Discussion started: 6 October 2025
Revised: 28 January 2026 – Accepted: 16 February 2026 – Published: 6 March 2026

Abstract. The EUCFe cruise (RV *Kilo Moana*, 2006) was designed to characterize sources of Fe to the western equatorial Pacific and its transport by the Equatorial Undercurrent (EUC), a narrow and fast eastward current flowing along the equator, to the eastern equatorial Pacific High Nutrient Low Chlorophyll (HNLC) region. This study presents seawater dissolved (DFe) and particulate (PFe) iron concentrations and isotopic compositions (δ^{56}DFe and δ^{56}PFe) from 15 stations in the equatorial band (2° N–2° S) between Papua New Guinea and 140° W, over more than 8500 km along the equator and in the upper 1000 m of the water column.

δ^{56}DFe and δ^{56}PFe ranged from -0.22 ‰ to $+0.79 \pm 0.07$ ‰ and from -0.52 ‰ to $+0.43 \pm 0.07$ ‰, respectively (relative to IRMM-14, 95 % confidence interval). Source signatures, biogeochemical processes and transport all contribute to these observations. Two distinct areas, one under continental influence (the western equatorial Pacific) and an open ocean region (the central equatorial Pacific), emerged from the data. In the area under continental influence, high PFe concentrations along with δ^{56}DFe values systematically heavier than that of δ^{56}PFe indicated an equilibrium fractionation and the co-occurrence of chemical fluxes from both phases toward the other. This exchange occurs through non-reductive processes, as previously proposed from three of the eight stations of this area (Labatut et al., 2014) and extends up to 1200 km from the coast. In the open ocean area, preservation of a DFe isotopic signature of $\sim +0.36$ ‰ within the EUC, from Papua New Guinea to the central equatorial Pacific (7800 km), confirmed the origin of the DFe carried within this current toward the HNLC region. At the same depth, bordering the EUC at 2° N and 2° S at 140° W, light isotopic signatures suggested that iron was originating from the eastern Pacific oxygen minimum zones. These light signatures were also observed in deeper central waters, between 200 and 500 m. Our data did not allow conclusions about fractionation during uptake by phytoplankton, but indicated that any fractionation, if present, must be small, no larger than a few tenths of a per mil.

1 Introduction

Iron (Fe) is an essential nutrient for phytoplankton, enabling them to fulfil their role as primary producers (Morel et al., 2020). Through its influence on primary productivity and plankton speciation, Fe plays a critical role in regulating the biological carbon pump and, consequently, the global carbon cycle and climate. Fe concentrations in the surface open ocean are often low (of the order of 0.1 nmol kg^{-1}), potentially limiting primary productivity (Martin, 1992). Regions where Fe is limiting, despite the availability of macronutrients, are termed High Nutrient Low Chlorophyll (HNLC) areas. One notable HNLC region is the eastern equatorial Pacific (Chisholm and Morel, 1991), where Fe is believed to have a main source from the western Pacific and to be transported eastward within the Equatorial Undercurrent (EUC) (Murray et al., 1994; Coale et al., 1996; Mackey et al., 2002; Kaupp et al., 2011). The EUC is an eastward-flowing subsurface current associated with upwellings that transports Fe from Papua New Guinea (PNG) toward South America along the equator (Gordon et al., 1997; Kaupp et al., 2011; Radic et al., 2011; Slemons et al., 2012; Winckler et al., 2016). Iron within the EUC is assumed to have both lithogenic and hydrothermal origins (Gordon et al., 1997). Specifically, the lithogenic component is suggested to primarily originate from rivers and sediments on the PNG continental margin

(Mackey et al., 2002; Slemons et al., 2010; Radic et al., 2011; Labatut et al., 2014).

Although Fe concentration data are fundamental, isotopic measurements provide deeper insight into both the provenance of Fe and internal processes governing its cycling (Lacan et al., 2008; John et al., 2012; Conway and John, 2014; Ellwood et al., 2015). The isotopic composition of Fe, expressed as δ^{56}Fe in per mil (‰), is defined as the deviation of the ^{56}Fe/^{54}Fe ratio of a sample from that of the IRMM-14 standard:

$$\delta^{56}\mathrm{Fe} = \frac{\left(^{56}\mathrm{Fe}/^{54}\mathrm{Fe}\right)_{\mathrm{sample}}}{\left(^{56}\mathrm{Fe}/^{54}\mathrm{Fe}\right)_{\mathrm{IRMM\text{-}14}}} - 1 \quad (1)$$

The isotopic signatures can trace Fe from distinct sources, including fluvial inputs (Fantle and DePaolo, 2004; Bergquist and Boyle, 2006; Ingri et al., 2006), sedimentary inputs (Severmann et al., 2006; Homoky et al., 2009; Radic et al., 2011; Labatut et al., 2014), hydrothermal inputs (Sharma et al., 2001; Severmann et al., 2004; Rouxel et al., 2008; Bennett et al., 2009), and atmospheric inputs (Waeles et al., 2007; Flament et al., 2008; Kurisu et al., 2016; Camin et al., 2025). They also provide information on internal oceanic processes. Processes such as biological assimilation, dissolution, sorption, precipitation, complexation and redox reactions, can modify the isotopic composition of Fe, through isotopic fractionation.

Despite advances, substantial uncertainties remain regarding both the isotopic signature of sources and the isotopic fractionation of processes. Hydrothermal and sedimentary sources are poorly characterized due to limited understanding of the processes governing Fe exchange and speciation. Additionally, the extent and mechanisms of isotopic fractionation remain incompletely understood. For example, fractionation caused by phytoplankton during biological uptake remains uncertain, with studies suggesting preferential uptake of either lighter or heavier isotopes (Lacan et al., 2008; Radic et al., 2011; Conway and John, 2014; Ellwood et al., 2015, 2020; Klar et al., 2018; Sieber et al., 2021; Tian et al., 2023; John et al., 2024).

To better understand the sources, transport, and cycling of Fe in this region, the EUCFe cruise (Equatorial Undercurrent Fe cruise) was conducted across the western and central equatorial Pacific (RV *Kilo Moana*, PI: J. W. Murray, 2006). Iron isotope data from the EUCFe cruise were previously published from four stations: three located in the west near PNG and one in the open ocean (0°, 180° E) (Radic et al., 2011; Labatut et al., 2014). At the three stations near PNG, an important source of dissolved Fe (DFe) was attributed to non-reductive exchange processes between dissolved and mainly lithogenic particulate phases. The Fe isotope signatures observed at the open ocean station indicated that in the deeper layer of the EUC the Fe isotope signatures from the western Pacific were preserved toward the open ocean over more than 4000 km. The Fe isotopic composition of aerosols, collected during the cruise, was also documented. Their slightly heavy signatures, δ^{56}PFe $= +0.31 \pm 0.21$ ‰ (2 SD, $n = 9$), were interpreted as reflecting isotopic fractionation due to partial dissolution of crustal dust during atmospheric transport (Camin et al., 2025).

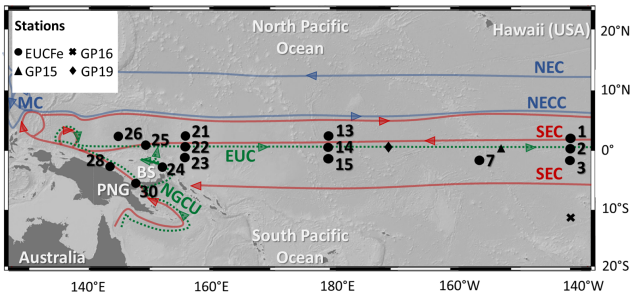

Figure 1. Map of the EUCFe stations and some GP15, GP16 and GP19 stations. Main surface and subsurface currents are represented, in blue those carrying water masses of northern origins, in red those carrying waters of southern origins and in dashed green the undercurrents. BS: Bismarck Sea; EUC: Equatorial UnderCurrent; MC: Mindanao Current; NEC: North Equatorial Current; NECC: North Equatorial CounterCurrent; NGCU: New Guinea Coastal Undercurrent; SEC: South Equatorial Current (Delcroix et al., 1992; Fine et al., 1994; Kashino et al., 1996, 2007; Johnson et al., 2002; Tomczak and Godfrey, 2003).

This present study reports Fe isotopic data from an additional 11 stations from the EUCFe cruise in the equatorial band (2° N–2° S) between Papua New Guinea and 140° W, over more than 8500 km along the equator and in the top 1000 m of the water column. By expanding the spatial coverage of concentration and isotopic measurements, we constrain the basin scale Fe biogeochemical cycle in the western and central equatorial Pacific.

2 Hydrodynamical context, water masses and currents

Seawater samples ($n = 76$) were collected during the EUCFe cruise from the surface to 1000 m depth in the western and central equatorial Pacific Ocean. This area is influenced by the South and the North Pacific subtropical gyres that shape the large-scale circulation. The equatorial branches of those gyres are westward currents extending from the surface to approximately 400 m depth (Cravatte et al., 2017): the North Equatorial Current (NEC) and the South Equatorial Current (SEC). The main surface and subsurface currents and the EUCFe stations with δ^{56}Fe data are represented in Fig. 1.

One of the specific structures of this circulation is the Equatorial Undercurrent (EUC). It is an intense subsurface equatorial current, with velocities up to 1 m s^{-1} (Philander, 1973), flowing along the equator over 14 000 km (Tomczak and Godfrey, 2003). Its core rises toward the surface eastward, from an average depth of 200 m in the western equatorial Pacific, to depths of 130 m in the central equatorial

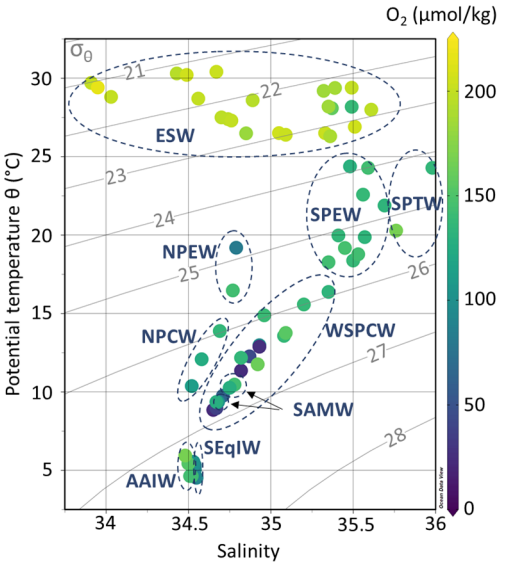

Figure 2. Potential temperature (θ, °C), salinity (S), dissolved oxygen concentrations (O_2, µmol kg^{-1}) of EUCFe samples. Isopycnals are shown in gray lines (σ_θ, kg m^{-3}). The dashed ellipses show water masses: Equatorial Surface Water (ESW), South Pacific Tropical Water (SPTW), South Pacific Equatorial Water (SPEW), North Pacific Equatorial Water (NPEW), Western South Pacific Central Water (WSPCW), North Pacific Central Water (NPCW), South Antarctic Mode Water (SAMW), South Equatorial Intermediate Water (SeqIW) and Antarctic Intermediate Water (AAIW).

Pacific and 40 m in the eastern equatorial Pacific (Tomczak and Godfrey, 2003; Talley et al., 2011). It is fed by waters from the Low-Latitude Western Boundary Currents (LLWBCs) composed at two-thirds by southern currents (New Guinea Coastal Current, New Guinea Coastal Undercurrent, New Ireland Coastal Undercurrent) and at one-third by northern currents (Mindanao Current) (Tsuchiya et al., 1989; Butt and Lindstrom, 1994; Fine et al., 1994; Rodgers et al., 2003; Grenier et al., 2011). The EUC is therefore enriched with nutrients of continental origins and plays an essential role supplying the eastern equatorial Pacific HNLC area through the equatorial upwelling (Coale et al., 1996; Ryan et al., 2006; Slemons et al., 2009; Kaupp et al., 2011).

Below the EUC, there is a westward subsurface flow, the Equatorial Intermediate Current (EIC). The EIC is bounded by eastward North and South Subsurface Countercurrents (NSCC and SSCC) centered around 2° N and 2° S, not shown in Fig. 1 (Tomczak and Godfrey, 2003; Cravatte et al., 2017).

In the equatorial Pacific Ocean between 140° E and 140° W, at least 9 different water masses can be observed in the upper 1000 m of the water column. Their θ, S and [O_2] characteristics are shown in Fig. 2 and reported in Table 1. The upper 100 m are mainly composed of the Equatorial Surface Water (ESW), characterized by high temperatures and oxygen concentrations. ESW is mainly formed from two water masses (Tropical Surface Water (TSW) and Subtropical Surface Water (STSW)). Those are formed in the tropics where evaporation exceeds precipitation and then transported toward the equator by the North and South subtropical gyres. Due to mixing with upwelled waters, ESW is colder than TSW and STSW (Fiedler and Talley, 2006). Between 100 and 200 m, there are three water masses, from the saltiest to the freshest: the South Pacific Tropical Water (SPTW), the South Pacific Equatorial Water (SPEW), the North Pacific Equatorial Water (NPEW) (Tsuchiya et al., 1989; Lacan and Jeandel, 2001; Grenier et al., 2013). The SPTW originates from surface waters subduction in the tropical South Pacific, a high-salinity area with excess evaporation (Tsuchiya et al., 1989). The SPEW is a less salty version of the SPTW and the prevailing water mass around the equator at these depths. It is the major constituent of the upper part of the EUC ($\sigma_\theta <$ 25.6 kg m^{-3}) (Lacan and Jeandel, 2001; Tomczak and Godfrey, 2003; Grenier et al., 2011; Grenier, 2012). The NPEW is formed by mixing of the SPEW and the North Pacific Central Water (NPCW) (Tomczak and Godfrey, 2003). Between 200 and 500 m depth, central waters, defined by a linear region on temperature-salinity diagrams, are found (Pollard et al., 1996; Stramma and England, 1999; Tomczak and Godfrey, 2003). The Western South Pacific Central Water (WSPCW), formed in the subtropical convergence zone between Tasmania and New Zealand, is the major constituent of the lower part of the EUC ($\sigma_\theta >$ 25.6 kg m^{-3}) (Tomczak and Hao, 1989; Grenier et al., 2011; Grenier, 2012). WSPCW is also the predominant water mass at these depths in the study area. The North Pacific Central Water (NPCW) is formed in the northern subtropical front (Tomczak and Godfrey, 2003). NPCW is found in the northern part of the study area. Between 350 and 600 m, there is also the South Antarctic Mode Water (SAMW), a water mass formed by vertical convective overturning at the end of the winter north of the Antarctic Circumpolar Current (McCartney, 1977; Sokolov and Rintoul, 2000). The SAMW is often associated with the Antarctic Intermediate Water (AAIW), a deeper water mass. Both water masses, SAMW and AAIW, are found in the western part of the study area. Between 600 and 1000 m, two intermediate waters can be identified: the Equatorial Intermediate Water (EqIW) and the AAIW. Some scientists refer to EqIW as part of the Antarctic Intermediate Water (AAIW) (Yuan and Talley, 1992; Talley, 1999, 2008; Qu and Lindstrom, 2004). In this article, the distinction between the EqIW and AAIW is relevant for studying key parameters such as oxygen, nutrient concentrations and salinity along the equator. The AAIW is formed by subduction of fresh surface water at the subantarctic front, west of the Drake Passage (Tsuchiya, 1991; Talley et al., 2011). The EqIW is a mixing of AAIW and Pacific Deep Water (formed without contact with the atmosphere by Antarctic Bottom Water, Atlantic Deep Water and AAIW mixing) (Tomczak and Godfrey, 2003; Bostock et al., 2010). It constitutes the predominant water mass at these depths in the study region.

https://doi.org/10.5194/os-22-791-2026

Table 1. Water masses identified during the EUCFe cruise, with their characteristics in the study area: origin, depth, potential temperature (θ, °C), salinity, potential density anomaly (σ_θ, kg m^{-3}) and dissolved oxygen concentration (O_2, µmol kg^{-1}). Where the currents flow is specified. Currents acronym meanings are available in Fig. 1, except for the North Equatorial Subsurface Current (NESC), the South Equatorial Subsurface Current (SESC) and the New Ireland Coastal Undercurrent (NICU).

Water Masses	Origin	EUCFe zone	Depth (m)	θ (°C)	Salinity	σ_θ (kg m^{-3})	O_2 (µmol kg^{-1})	Currents	Characteristics	References
Equatorial Surface Water (ESW)	Mixing between the Tropical Surface Water and the Subtropical Surface Water, equatorial upwellings, advection of the Peru Current Water	Entire zone	0–100	21.0–30.5	33.5–35.7	20.5–23.5	108–193	SEC, NGCC, NICU, EUC	/	Fiedler and Talley (2006); EUCFe sensor data
South Pacific Tropical Water (SPTW)	Subduction of surface waters in the tropics in a high-salinity area (evaporation excess) around the Polynesian region	Southeastern stations (stations 3 and 15)	100–200	18–25	35.7–36.7	24.3–25.3	134–167	SEC, NGCU, NGCC, NICU, EUC	Subsurface salinity maximum	Tsuchiya et al. (1989); Qu and Lindstrom (2002); EUCFe sensor data
South Pacific Equatorial Water (SPEW)	Subduction of surface waters in the tropics in a high-salinity area (evaporation excess) around the Polynesian region: one branch, less salty, of the SPTW	Mainly western equatorial and southwestern stations	100–200	18–25	35.3–35.8	23.8–25.6	129–145	SEC, NICU, NGCU, NGCC, EUC	/	Tomczak and Hao (1989); Tsuchiya et al. (1989); Qu and Lindstrom, 2002; Tomczak and Godfrey (2003); EUCFe sensor data
North Pacific Equatorial Water (NPEW)	Mixture between SPEW and NPCW	Northern stations (stations 1 and 26)	100–200	16–20	34.7–35.0	24.3–25.5	80–145	NEC, EUC	Salinity minima of tropical waters	Tomczak and Godfrey (2003); EUCFe sensor data
North Pacific Central Water (NPCW)	Northern subtropical front	Northwestern stations (stations 13, 21, 26)	200–300	10–17	33.5–34.7	25.2–26.4	110–135	EUC	Salinity minima of central waters	Emery and Meincke (1986); Pickard and Emery (1990); Tomczak and Godfrey (2003); Grenier (2012); EUCFe sensor data

Table 1. Continued.

Water Masses	Origin	EUCFe zone	Depth (m)	θ (°C)	Salinity	σ_θ (kg m^{-3})	O_2 (µmol kg^{-1})	Currents	Characteristics	References
Western South Pacific Central Water (WSPCW)	Subtropical convergence zone between Tasmania and New Zealand	Equatorial and southern stations and some northern stations	170–500	8.9–17	34.7–35.5	26.1–26.9	20–160	SEC, NGCU, NICU, EUC, EIC, NSCC, SSCC	Salinity maximum of central waters	Tsuchiya (1981); Tomczak and Hao (1989); Tsuchiya et al. (1989); Sokolov and Rintoul (2000); Qu and Lindstrom (2002); Tomczak and Godfrey (2003); Qu et al. (2009); Grenier (2012); EUCFe sensor data
South Antarctic Mode Water (SAMW)	Vertical convective overturning at the end of winter north of the Antarctic Circumpolar Current	Western stations (stations 22, 24, 25)	350–600	8.0–9.5	34.6–34.75	26.7–26.9	100–145	EIC, SEC	/	McCartney (1977); Sokolov and Rintoul (2000); EUCFe sensor data
South Equatorial Intermediate Water (SEqIW)	Mixing of AAIW and Pacific Deep Water	Every sample between 700 and 1000 m depth except the Southernmost stations close to the Bismarck Sea	700–1000	4.4–5.6	34.5–34.6	27.2–27.4	80–105	EIC, NSCC, SSCC, NESC, SESC	/	Wyrtki (1962); Bingham and Lukas (1995); Bostock et al. (2010); EUCFe sensor data
AntArctic Intermediate Water (AAIW)	Subduction of fresh surface water at the subantarctic front, west of the Drake Passage	Southernmost stations in the Bismarck Sea: at less than 60 km from Papua New Guinea coast (stations 24, 28, 30)	700–1000	4.7–6.0	34.4–34.6	27.2–27.3	140–170	SEC, NGCU, NGCC, NICU	Salinity minima of intermediate waters	Tsuchiya (1991); Tsuchiya and Talley (1996); Talley et al. (2011); EUCFe sensor data

3 Sampling and analytical procedures

Sampling and analytical procedures have been previously described (Radic et al., 2011; Labatut et al., 2014). They are summarized below.

Seawater was sampled from surface to 1000 m depth using acid cleaned Go-Flo bottles (12 L) mounted on a trace metal rosette equipped with a CTD, lent by the University of Victoria (Canada). Sample filtration was performed onboard in a homemade plastic room pressurized with filtered air, with acid-cleaned Nuclepore™ membranes (0.4 µm pore size, 90 mm diameter) housed in Teflon filter holders (Savillex™). After filtration, 10 L of filtered seawater were stored in acid-cleaned polyethylene containers and membranes were stored in acid-cleaned Petri dishes.

Samples were processed and analyzed at the LEGOS laboratory (Observatoire Midi-Pyrénées, Toulouse, France) between 2009 and 2012. All chemical procedures were conducted in a trace-metal-clean laboratory under an ISO4 laminar flow hood, using high purity reagents and acid cleaned labware.

Particles were fully digested in a mixture of 5 M HCl, 2.1 M HNO_3, and 0.6 M HF at 130 °C for 3 h. To verify the completeness of the digestion, selected filters were re-digested, confirming no particulate Fe (PFe) remained. Aliquots (2 %) were reserved for Al concentration measurements using an Element-XR HR-ICP-MS. A ^{57}Fe-^{58}Fe double spike was added to the remaining 98 % of the digested material and to filtered seawater, in preparation for isotopic analyses. Dissolved iron was preconcentrated from filtered seawater on a NTA Superflow resin, at pH = 1.8. Fe was purified from both types of samples with AG1-X4 anionic resin. Iron isotopic compositions and concentrations were measured with a Neptune MC-ICP-MS.

Uncertainties are reported at a 95 % confidence level throughout this article. For Fe concentrations and isotope measurements on the Neptune, the total procedural recovery was 93 ± 25 % for PFe and 86 ± 33 % for DFe. The total procedural blanks were 0.74 ± 1.17 ng (2 SD) for DFe and 7.47 ± 1.09 ng (2 SD) for PFe. This amounts to 0.5 % and 0.6 % of the samples' average Fe content for DFe and PFe, respectively and 2.8% and 9.7 % for the sample with the smallest Fe content for DFe and PFe, respectively. For DFe, the filtered seawater from a sample was divided into several aliquots, then each was processed individually (including different double spiking, preconcentration and purification). For PFe, each sample, i.e., membrane, was first digested (no division of the membrane before digestion), then the digested sample was divided into several aliquots, and each was processed individually (including different double spiking and purification). In some instances, duplicate samples are taken at sea, from the same cast. These replicates are termed "Go-Flo replicates" in the Table A1 in the Appendix. Repeatability was 8 % for DFe concentrations, 4 % for PFe concentrations, 0.05 ‰ for δ^{56}DFe and 0.04 ‰ for δ^{56}PFe. This level of precision is better than the long-term external precision of 0.07 ‰, determined from repeated analyses of an in-house "ETH Hematite" isotopic standard. As a result, uncertainties for δ^{56}Fe data are reported as either ± 0.07 ‰ or the internal measurement uncertainty (2 standard errors), whichever is larger.

The LEGOS Fe isotope protocol has been validated through intercalibration and intercomparison exercises (Boyle et al., 2012; Conway et al., 2016) and detailed in Lacan et al. (2008, 2010, 2021). Accuracy (referring to the two concepts of trueness and precision) of elemental concentrations measured by HR-ICP-MS was regularly verified using the certified SLRS-5 river water material and through intercalibration exercises (Yeghicheyan et al., 2013, 2019).

4 Results

Concentrations and isotopic compositions of DFe and PFe in seawater are reported in Table 2. Previously published data from four stations (14, 24, 28 and 30) are included here for clarity (Radic et al., 2011; Labatut et al., 2014). All Fe concentrations, Fe isotopic compositions, temperature, salinity, oxygen data and an intercalibration report, have been included in the GEOTRACES Data Product. They are also available on the SEANOE open data repository (Lacan et al., 2025).

Two distinct groups of stations emerge from these observations. These are the western equatorial Pacific and central equatorial Pacific. In the western equatorial Pacific, PFe concentrations were significantly higher, approximately seven times larger, than typical open ocean values. This group includes stations 21, 22, 23, 24, 25, 26, 28 and 30. In the central equatorial Pacific, PFe concentrations were mostly typical of open ocean values. This group includes stations 1, 2, 3, 7, 13, 14 and 15. Data for both areas are shown in Figs. 3 and 4.

4.1 Iron concentrations

DFe and PFe concentrations ranged from 0.05 to 1.46 nmol kg^{-1} and from 0.14 to 29.45 nmol kg^{-1}, respectively.

A few common features in Fe concentration profiles can be identified across stations from the surface to 1000 m. (i) With the exception of station 28 located near the mouth of the Sepik River, lowest concentrations were found near the surface, mostly in the chlorophyll maximum layer, where biological uptake depletes the concentration of bioavailable Fe. (ii) From the surface to 200 m depth, Fe concentrations tended to increase. Deeper than 200 m, the profiles became more variable, with no uniform trend across stations. (iii) Stations 3, 13, 14 and 15 displayed typical open ocean, nutrient like, DFe profiles. (iv) The particulate iron (PFe) fraction predominated over the dissolved fraction (DFe), accounting on average for 80 % mol mol^{-1} of total iron (TFe) at western

Table 2. Location, depth, hydrological properties, concentration and isotopic composition of dissolved and particulate Fe (DFe and PFe). Concentration relative uncertainties are 8.0 % for DFe and 4.3 % for PFe (95 % confidence level). U95 stands for measurement uncertainty at the 95 % confidence level. For most samples, dissolved O_2 concentration was measured in the samples onboard. When direct measurements were not available, as indicated by the superscripted "a", oxygen concentrations from the oxygen sensor on the rosette were used following calibration with in situ data. The superscripted "b" and "c" indicate data previously published by Radic et al. (2011) and Labatut et al. (2014), respectively. ESW: Equatorial Surface Water; SPTW: South Pacific Tropical Water; SPEW: South Pacific Equatorial Water; NPEW: North pacific Equatorial Water; NPCW: North Pacific Central Water; WSPCW: Western South Pacific Central Water; SAMW: South Antarctic Mode Water; SEqIW: South Equatorial Intermediate Water; AAIW: Antarctic Intermediate Water; Chloro. Max: Chlorophyll Maximum layer.

GoFlo bottle	Depth (m)	θ (°C)	Salinity	O_2 (μmol kg^{-1})	σ_θ (kg m^{-3})	Water mass	DFe (nmol kg^{-1})	δ^{56}DFe (‰)	δ^{56}DFe U95 (‰)	PFe (nmol kg^{-1})	δ^{56}PFe (‰)	δ^{56}PFe U95 (‰)
STATION 1 (1.6° N 140.0° W, cast TM3, 25 August 2006, bottom depth: 4364 m)												
12	15	26.5	35.05	204	22.93	ESW	0.26	+0.43	0.08	0.39	+0.06	0.07
10	48	26.4	35.09	202	22.98	ESW (Chloro. Max.)	0.26	+0.32	0.07	0.43	+0.25	0.07
8	119	19.2	34.79	81	24.82	NPEW	0.37	+0.28	0.08	0.24	+0.23	0.07
6	268	12.3	34.87	43	26.43	WSPCW	0.36	−0.19	0.11	0.21	+0.06	0.07
4	497	8.8	34.65	[a]23	26.88	WSPCW	0.71	−0.22	0.09	0.38	+0.12	0.07
2	794	5.3	34.54	[a]87	27.28	SEqIW	0.77	+0.40	0.07	0.30	−0.11	0.07
STATION 2 (0.0° N 140.0° W, cast TM9, 26 August 2006, bottom depth: 4333 m)												
12	15	26.5	35.33	201	23.13	ESW	0.13	+0.19	0.07	0.47	+0.19	0.07
10	49	26.2	35.36	188	23.23	ESW (Chloro. Max.)	0.38	+0.14	0.09	–	–	–
8	114	24.3	35.59	143	24.00	SPEW	0.17	+0.25	0.07	–	–	–
6	246	13.0	34.93	98	26.34	WSPCW	0.44	+0.29	0.07	–	–	–
4	348	11.4	34.82	[a]24	26.57	WSPCW	0.43	−0.10	0.07	–	–	–
2	992	4.6	34.55	[a]86	27.37	SEqIW	0.61	+0.11	0.07	–	–	–
STATION 3 (2.0° S 139.6° W, cast TM11, 27 August 2006, bottom depth: 4257 m)												
12	13	26.9	35.51	203	23.13	ESW	0.07	–	–	0.60	+0.41	0.07
10	59	26.9	35.51	205	23.14	ESW (Chloro. Max.)	0.06	+0.31	0.07	–	–	–
8	110	20.3	35.76	167	25.25	SPTW	0.14	+0.30	0.12	0.14	+0.33	0.07
7	198	12.8	34.93	25	26.37	WSPCW	0.24	−0.06	0.07	–	–	–
4	476	9.0	34.67	[a]36	26.87	SEqIW	0.43	+0.14	0.07	–	–	–
1–2	993	4.5	34.55	[a]91	27.37	SEqIW	0.41	+0.35	0.07	0.40	+0.15	0.08
STATION 7 (2.1° S 155.1° W, cast TM16, 2 September 2006, bottom depth: 4992 m)												
11	75	27.9	35.61	196	22.87	ESW (Chloro. Max.)	0.07	–	–	0.55	+0.22	0.07
STATION 13 (2.0° N 179.6° W, cast TM25, 10 September 2006, bottom depth: 5218 m)												
12	15	30.3	34.43	195	21.20	ESW	0.07	+0.79	0.07	0.80	−0.04	0.08
10	79	29.2	35.32	184	22.23	ESW (Chloro. Max.)	0.10	+0.35	0.07	0.49	+0.26	0.11
8	119	28.2	35.49	137	22.69	ESW	0.07	+0.72	0.07	–	–	–
7	170	13.8	34.69	134	25.98	NPCW	0.32	+0.30	0.08	0.87	+0.12	0.10
4	377	10.3	34.75	[a]68	26.70	WSPCW	0.47	+0.35	0.07	1.02	+0.12	0.12
2	892	5.1	34.54	97	27.30	SEqIW	0.41	+0.25	0.07	0.31	–	–

Table 2. Continued.

GoFlo bottle	Depth (m)	θ (°C)	Salinity	O_2 (μmol kg^{-1})	σ_θ (kg m^{-3})	Water mass	DFe (nmol kg^{-1})	δ^{56}DFe (‰)	δ^{56}DFe U95 (‰)	PFe (nmol kg^{-1})	δ^{56}PFe (‰)	δ^{56}PFe U95 (‰)
STATION 14 (0.0° N 180° E, cast TM28, 11 September 2006, bottom depth: 5260 m)[b]												
12	14	30.4	34.67	201	21.35	ESW	0.06	–	–	0.37	+0.27	0.07
10	98	29.4	35.39	186	22.22	ESW (Chloro. Max.)	0.06	+0.58	0.07	0.43	+0.43	0.09
8	139	22.6	35.56	137	24.48	SPEW	0.20	+0.31	0.08	0.53	+0.13	0.09
6	197	14.9	34.86	140	25.88	WSPCW	0.53	+0.40	0.12	0.53	+0.40	0.07
4	397	9.8	34.71	64	26.76	WSPCW	0.61	+0.01	0.07	0.81	+0.15	0.11
2	842	5.3	34.54	82	27.27	SEqIW	0.59	+0.22	0.08	0.51	+0.28	0.10
STATION 15 (2.0° S 180.0° E, cast TM30, 12 September 2006, bottom depth: 5390 m)												
12	16	30.2	34.49	206	21.27	ESW	0.06	+0.55	0.07	0.39	+0.27	0.07
10	75	29.3	35.49	199	22.32	ESW (Chloro. Max.)	0.05	–	–	0.27	+0.30	0.07
8	139	24.2	35.98	134	24.31	SPTW	0.10	+0.43	0.07	0.33	+0.23	0.12
6	171	16.4	35.35	133	25.93	WSPCW	0.23	+0.20	0.07	0.49	+0.12	0.11
2	844	5.3	34.53	99	27.27	SEqIW	0.58	+0.32	0.07	0.98	−0.05	0.10
STATION 21 (2.0° N 156.0° E, cast TM40, 20 September 2006, bottom depth: 2587 m)												
10	75	28.1	35.37	158	22.65	ESW (Chloro. Max.)	0.11	–	–	0.41	+0.18	0.14
8	147	24.4	35.48	129	23.89	SPEW	0.36	+0.40	0.08	0.60	−0.05	0.07
7	194	12.0	34.58	124	26.25	NPCW	0.45	+0.16	0.07	1.59	+0.05	0.07
STATION 22 (0.2° N 156.0° E, cast TM43, 21 September 2006, bottom depth: 2049 m)												
12	24	29.7	33.91	200	21.00	ESW	0.09	–	–	0.39	+0.19	0.07
10	54	28.6	34.89	195	22.12	ESW (Chloro. Max.)	0.09	–	–	0.32	+0.22	0.07
8	191	18.2	35.35	143	25.49	SPEW	0.71	+0.48	0.08	2.89	+0.00	0.07
6	257	12.2	34.82	134	26.41	WSPCW	0.96	+0.40	0.07	4.26	+0.02	0.07
4	393	9.3	34.68	[a]101	26.82	SAMW	–	–	–	1.51	+0.01	0.12
3	393	9.3	34.68	[a]101	26.82	SAMW	0.91	+0.25	0.07	1.68	+0.05	0.15
STATION 23 (1.2° S 155.6° E, cast TM45, 22 September 2006, bottom depth: 1997 m)												
10	74	28.2	35.35	[a]183	22.60	ESW (Chloro. Max.)	0.07	+0.26	0.09	0.29	+0.14	0.11
8	185	18.4	35.50	[a]138	25.56	SPEW	0.46	+0.32	0.09	1.83	−0.03	0.14
6	218	13.6	35.08	[a]137	26.34	WSPCW	0.72	+0.29	0.07	1.87	+0.04	0.07
5	218	13.6	35.08	[a]137	26.34	WSPCW	0.72	+0.30	0.11	2.52	−0.01	0.13
4	218	13.6	35.08	[a]137	26.34	WSPCW	0.75	+0.22	0.07	2.70	+0.03	0.12
STATION 24 (3.2° S 152.3° E, cast TM47, 23 September 2006, bottom depth: 1669 m)[c]												
11	39	28.7	34.56	199	21.83	ESW	0.48	−0.03	0.07	1.15	+0.13	0.14
9	64	27.4	34.74	196	22.38	ESW (Chloro. Max.)	0.30	+0.20	0.07	1.66	+0.01	0.16
7	179	19.9	35.57	133	25.22	SPEW	0.86	−0.03	0.07	7.81	−0.48	0.11
5	367	10.5	34.78	[a]143	26.70	WSPCW	0.67	+0.27	0.08	4.87	−0.03	0.12
2	912	4.6	34.52	141	27.34	AAIW	0.99	+0.34	0.07	4.91	+0.00	0.10

Table 2. Continued.

GoFlo bottle	Depth (m)	θ (°C)	Salinity	O_2 (μmol kg^{-1})	σ_θ (kg m^{-3})	Water mass	DFe (nmol kg^{-1})	δ^{56}DFe (‰)	δ^{56}DFe U95 (‰)	PFe (nmol kg^{-1})	δ^{56}PFe (‰)	δ^{56}PFe U95 (‰)
STATION 25 (0° N 149.3° E, cast TM50, 25 September 2006, bottom depth: 3364 m)												
11	25	29.4	33.95	215	21.14	ESW	0.17	–	–	0.44	+0.25	0.09
9	135	21.9	35.69	133	24.79	SPEW	0.70	+0.03	0.13	1.44	−0.52	0.10
6	198	15.6	35.20	136	26.00	WSPCW	0.75	+0.38	0.14	4.12	+0.02	0.07
5	372	10.3	34.75	[a]126	26.71	SAMW	0.99	–	–	3.48	+0.00	0.07
3	793	5.5	34.53	[a]103	27.24	SEqIW	0.98	+0.13	0.07	1.76	−0.06	0.07
2	793	5.5	34.53	[a]103	27.24	SEqIW	0.87	–	–	1.77	−0.05	0.07
STATION 26 (1.6° N 145.0° E, cast TM52, 26 September 2006, bottom depth: 4490 m)												
11	24	28.8	34.03	200	21.40	ESW	0.16	–	–	0.42	–	–
8	152	20.0	35.41	135	25.08	SPEW	0.61	–	–	2.20	+0.01	0.07
6	219	16.4	34.77	[a]144	25.48	NPEW	0.36	–	–	1.85	+0.12	0.07
5	258	10.4	34.52	[a]111	26.51	NPCW	0.64	+0.20	0.07	2.09	+0.04	0.07
3	346	9.4	34.67	[a]127	26.79	WSPCW	0.83	–	–	3.76	+0.02	0.07
STATION 28 (3.4° S 143.9° E, cast TM56, 28 September 2006, bottom depth: 2256 m)[b,c]												
10	39	27.5	34.70	196.6	22.32	ESW	0.89	+0.53	0.07	29.45	+0.04	0.09
8	94	26.5	34.85	180.9	22.77	ESW (Chloro. Max.)	0.45	+0.40	0.10	4.64	+0.01	0.07
7	189	19.1	35.45	145	25.33	SPEW	0.67	+0.43	0.11	6.91	+0.29	0.07
5	319	13.8	35.09	154	26.31	WSPCW	0.77	+0.29	0.07	7.34	+0.04	0.07
2	793	5.5	34.50	151	27.22	AAIW	1.46	+0.06	0.07	9.29	−0.03	0.10
STATION 30 (5.6° S 147.4° E, cast TM61, 30 September 2006, bottom depth: 1040 m)[c]												
10	23	27.3	34.76	[a]200	22.44	ESW	0.13	–	–	0.45	+0.30	0.11
7	199	18.7	35.53	[a]144	25.49	SPEW	0.65	+0.41	0.12	3.72	+0.17	0.07
6	348	11.8	34.92	[a]162	26.57	WSPCW	0.48	+0.31	0.07	3.90	+0.20	0.07
3	724	5.9	34.48	[a]166	27.15	AAIW	0.94	+0.44	0.12	3.23	+0.01	0.07
2	909	4.6	34.51	[a]143	27.33	AAIW	1.21	–	–	7.62	−0.03	0.07

equatorial Pacific stations (140–156° E) and 66 % mol mol^{-1} at central equatorial Pacific stations (180° E–140° W) (Fig. A1 in the Appendix).

Slemons et al. (2010, 2012) measured DFe and PFe concentrations by FIA during the same cruise. All data were of the same order of magnitude and ranged similarly. However, our data were almost systematically slightly lower (with a mean difference of 0.35 ± 0.44 nmol kg^{-1} for DFe and 0.35 ± 0.90 nmol kg^{-1} for PFe). In addition, EUCFe DFe and PFe concentration data are in good agreement with data published in the same area (John et al., 2018; Marsay et al., 2018; Zheng and Sohrin, 2019; Cohen et al., 2021; Sarthou et al., 2025).

4.2 Iron isotopic compositions

The isotopic signatures of dissolved (δ^{56}DFe) and particulate Fe (δ^{56}PFe) ranged from −0.22 ‰ to +0.79 ‰ and −0.52 ‰ to +0.43 ‰, respectively (Fig. 4).

Across all stations, 85 % of the samples had isotopic compositions of dissolved iron (δ^{56}DFe) higher than the upper continental crust (UCC) reference value of +0.07 ‰ (Poitrasson, 2006). δ^{56}DFe of western equatorial Pacific stations ranged from −0.03 ‰ to +0.53 ‰, with an average of $+0.28 \pm 0.30$ ‰ (2 SD, $n = 27$) and showed no systematic variation with depth or location. At the central equatorial Pacific stations, δ^{56}DFe ranged from −0.22 ‰ to +0.79 ‰, with an average of $+0.27 \pm 0.45$ ‰ (2 SD, $n = 32$). The surface layer exhibited relatively heavy isotopic signatures (around +0.5 ‰), which generally decreased with depth, reaching values around −0.2 ‰ at approximately 400 m. Below this depth, between 800 and 1000 m, δ^{56}DFe values increased again, to +0.4 ‰.

The isotopic compositions of particulate iron (δ^{56}PFe) at the western equatorial Pacific stations, $+0.03 \pm 0.32$ ‰ (2 SD, $n = 39$) on average, were remarkably homogeneous and remained close to the UCC value, except for two samples from stations 24 and 25. At the central equatorial Pacific stations, δ^{56}PFe were slightly more variable, from −0.11 ‰ to +0.43 ‰ (with an average of $+0.19 \pm 0.27$ ‰, 2 SD, $n = 26$), and 81 % of the samples were heavier relative to the UCC.

EUCFe data can be compared with three nearby cruises: GEOTRACES GP16 (2013), a zonal cruise along 10° S, from 75° W to 155° W, GEOTRACES GP15 (2018), a meridional section along 150° W with one station located at the equator

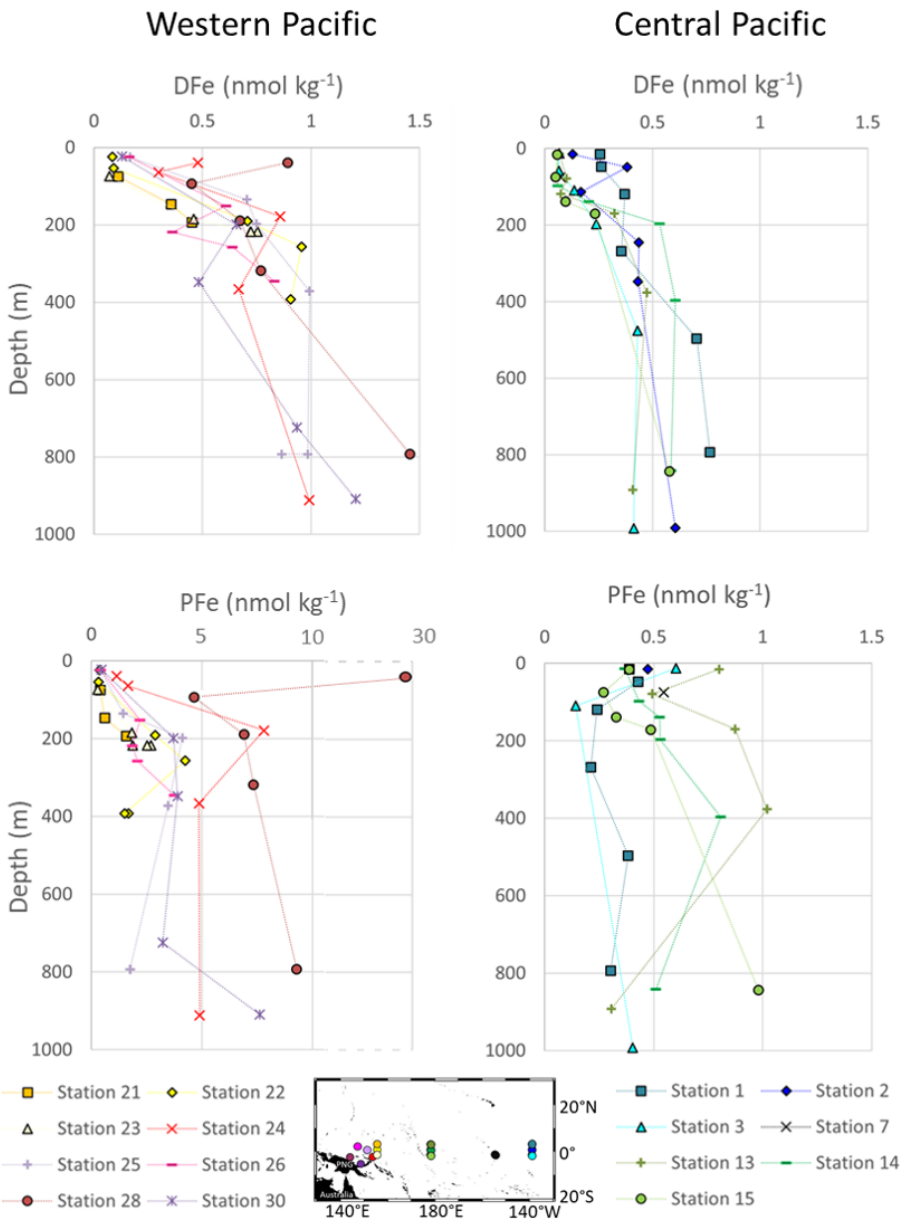

Figure 3. Profiles of concentrations of DFe and PFe in nmol kg^{-1} in the western equatorial and central equatorial Pacific. For each station, the error bars are smaller than the symbols for Fe concentrations: on average 8 % for DFe and 4 % for PFe. Stations 14 and 28 were previously published by Radic et al. (2011) and stations 24, 28 and 30 by Labatut et al. (2014). The x-axis is broken to show all PFe concentrations from western equatorial Pacific stations.

and GEOTRACES GP19 (2015), a meridional section along 170° W with one station located at the equator (Fig. 1). In the equatorial Pacific area, the circulation is highly zonal, and previous studies have shown that the water mass geochemistry at 12° S is not directly linked to that of the equatorial band (Lacan and Jeandel, 2001). This prevents the use of GP16 data and limits that of GP15 and GP19 to their equatorial stations (stations 29 and 21, respectively). These GP15 and GP19 Fe isotope data have not yet been published but are available in GEOTRACES Intermediate Data Product 2025 (GEOTRACES Intermediate Data Product Group, 2025). Figure 5 displays the GP15 station 29 and GP19 station 21 δ^{56}DFe profiles with the closest equatorial EUCFe stations, stations 2 and 14 (EUCFe station 7 is excluded from this comparison because it only reports a single data point at 75 m). Given the time lag between the three cruises (up to 12 years), and the thousand km between the stations, the upper 200 m are excluded from this comparison due to potential variabilities. At four depths, approximately 200, 400, 800 and 1000 m, δ^{56}DFe data from the three cruises can be com-

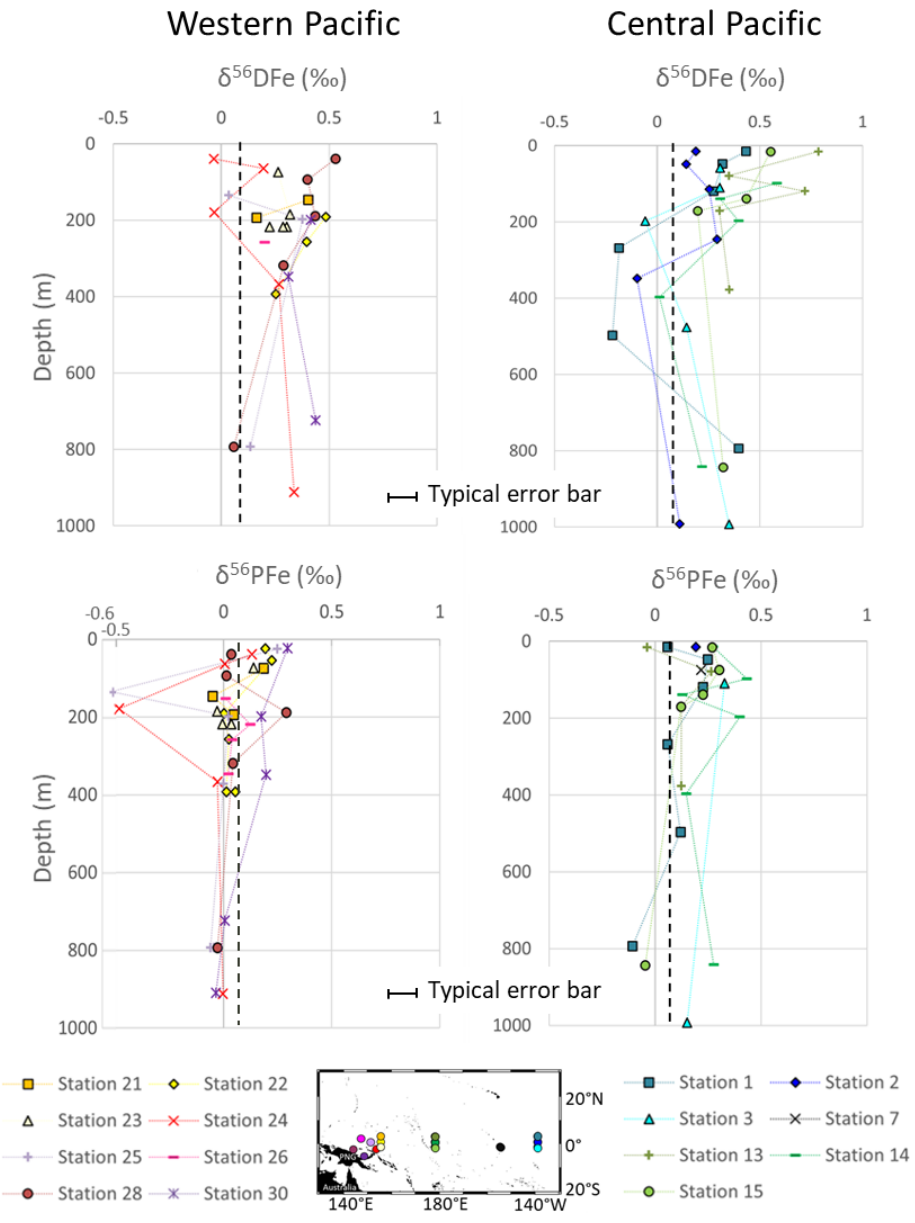

Figure 4. δ^{56}DFe and δ^{56}PFe profiles in the western equatorial and central equatorial Pacific. The black dashed line indicates the crustal value, +0.07 ‰ (Poitrasson, 2006). Individual error bars are not shown for clarity, but typical uncertainty (±0.07 ‰) is indicated by the scale bar.

pared (Fig. 5). These are in excellent agreement. No δ^{56}PFe data have been reported for GP15 and GP19.

5 Discussion

5.1 Influence of external iron inputs in the western equatorial Pacific

Fe concentrations throughout the entire water column in the western equatorial Pacific were approximately twice as high for DFe (0.63 nmol kg^{-1} compared to 0.30 nmol kg^{-1}, on average) and approximately seven times higher for PFe (3.58 nmol kg^{-1} compared to 0.49 nmol kg^{-1}, on average) relative to the central equatorial Pacific stations. The particulate Fe (PFe) fraction dominated total Fe (TFe), particularly in the western equatorial Pacific stations, where PFe/TFe ratios ranged from 63 % mol mol^{-1} to 97 % mol mol^{-1} (Fig. A1). These patterns were documented previously in several studies, and attributed to lithogenic inputs from terrestrial sources, with occasional hydrothermal contributions and minimal input from atmospheric sources (Milliman, 1995;

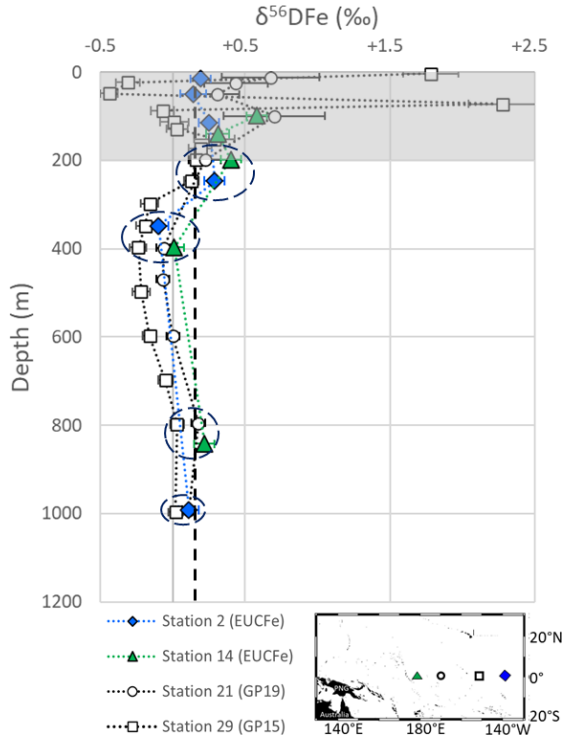

Figure 5. Comparison of δ^{56}DFe values from the EUCFe, GP15 and GP19 cruises. The upper 200 m, shaded in gray, are excluded from the comparison. The dashed ellipses show the 4 depths where comparison can be made for δ^{56}DFe values. Please note that at 1000 m, values from stations 2, 21 and 29 are close, making station 21 less visible. The black dashed line indicates the crustal value. The GP15 cruise data were produced by M. Sieber and T. Conway, and the GP19 cruise data were produced by Tim Conway, Matthias Sieber and Derek Vance; both datasets are available in the GEOTRACES Data product (GEOTRACES Intermediate Data Product Group, 2025).

Kineke et al., 2000; Mackey et al., 2002; Slemons et al., 2010; Radic et al., 2011; Labatut et al., 2014).

A box model (Fig. 6) for the region 133° E–177° W, 9° S–15° N was used to investigate the relative importance of possible PFe sources leading to these high concentrations. The model includes PFe transported by oceanic currents, atmospheric deposition and delivered by rivers (notably the Sepik River, with potential deposition to and resuspension from sediments). Particle settling within the water column and hydrothermal sources were neglected.

The transport of water masses in this area, from the surface to a depth of 1000 m, was estimated at 19.4 ± 0.4 Sv (1 SD), based on the flow in Vitiaz Strait during the Austral winter (i.e., the same period as the EUCFe cruise) (Germineaud et al., 2016). The incoming water is assumed to carry a typical open ocean PFe concentration (average value for the upper 1000 m of the water column, station 36, GP16 cruise) of 0.15 ± 0.08 nmol kg^{-1} (1SD) (Marsay et al., 2018), prior to enrichment within the study area (Fig. 1). The flux of PFe transported by water masses into this area, calculated as the product of these two quantities, is Flux $\mathrm{PFe}_{\mathrm{SW\,in}} = 14.5 \times 10^6$ g(PFe) d^{-1}. The average PFe concentration in this area (stations 21 to 30) ranged between 2.9 and 3.8 nmol kg^{-1} depending on the calculation method chosen (Table A1). The fluxes derived from these concentrations will be given as a range. This leads to a PFe flux transported out of the area by water masses, Flux $\mathrm{PFe}_{\mathrm{SW\,out}}$, between 272×10^6 and 357×10^6 g(PFe) d^{-1} (concentration multiplied by 19.4 Sv). In a steady state model, where inputs are balanced by outputs, one or more sources must be contributing approximately between 258×10^6 and 342×10^6 g(PFe) d^{-1} to this area.

Particulate iron atmospheric deposition was estimated using the Fe concentration in aerosols over this region, measured during the same cruise at 3.01 ng m^{-3} (Camin et al., 2025), multiplied by a bulk aerosol deposition velocity. The deposition area shown in Fig. 6, chosen as representative of this region of elevated PFe concentrations, covers approximatively 1.54×10^7 km^2 (the box model surface area of 1.6×10^7 km^2 minus the New Guinea land area of 0.08×10^7 km^2; Baldacchino, 2024). The bulk aerosol deposition velocity, denoted Vb (m d^{-1}), includes both wet and dry deposition. It can be calculated from the precipitation rate (mm d^{-1}) according to the formula from Kadko et al. (2020), recently updated by He et al. (2025), who used ^{7}Be as a proxy for atmospheric deposition:

$$\mathrm{Vb} = 413 \pm 22 \times \text{Precipitation Rate} + 1069 \pm 71 \qquad (2)$$

To estimate the precipitation rate, we used the NASA Giovanni data product TRMM to determine the mean daily precipitation rate over the entire region considered in the box model from 20 to 30 September 2006. The mean value was 11.4 ± 6.6 mm d^{-1} (2 SD) (Table A2). Applying Eq. (2), the bulk aerosol deposition velocity is therefore 5777 m d^{-1}. The resulting atmospheric PFe deposition flux was Flux $\mathrm{PFe}_{\mathrm{aerosol}} = 268 \times 10^6$ g(PFe) d^{-1}. This estimate accounts for between 78 % and 104 % of the required external sources (Table A1). However as discussed below, this PFe atmospheric deposition flux is orders of magnitudes lower than that delivered by rivers.

Papua New Guinea accounts for 8 % to 10 % of the global export of sediment to the ocean (1.7×10^{17} g(sediment) yr^{-1}) (Milliman et al., 1999). The Sepik River and other northern rivers of PNG discharge 8.6×10^{14} g(sediment) yr^{-1} to this study area (Milliman et al., 1999). Assuming that Fe amounts to 5 % w w^{-1} of the sediment discharge, (the UCC value from Rudnick and Gao, 2014), the estimated riverine discharge of PFe to the western equatorial Pacific is 4.3×10^{13} g(PFe) yr^{-1}, i.e., 1.2×10^{11} g(PFe) d^{-1}. This estimate accounts for between 35 064 % and 46 556 % of the required external sources (Table A1).

Thus, the riverine PFe flux is 448-fold larger than the atmospheric PFe flux. This flux comparison argues in favor of a contribution dominated by input from rivers. Isotopic signatures provide an additional constraint and also support a

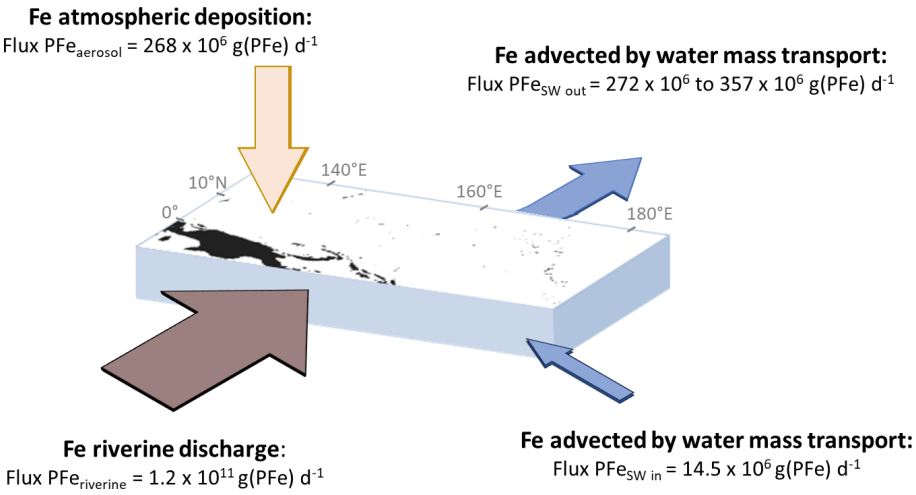

Figure 6. Box model describing PFe inputs and output to the western equatorial Pacific region. Note that although all external sources enter the seawater box, part of them are removed to the sediments.

riverine source, as the δ^{56}PFe values are close to crustal values in this region (Table 2 and Fig. 4), whereas aerosols exhibit a heavier isotopic signature, around +0.3 ‰ (Camin et al., 2025).

Regarding riverine particles, the question of their transport mechanism over such a distance from the coast (∼ 1200 km) arises. The Sepik River and other northern rivers of PNG deliver large sediment loads to the coastal ocean due to factors including intense rainfall from the Inter-Tropical Convergence Zone, a narrow shelf associated with the active margin, the sediment erodibility (geology, human activities) and tectonism (seismic and volcanic activity, relief) (Milliman and Syvitski, 1992). Lithogenic iron (Fe) observed at the western equatorial Pacific stations can be due to direct fluvial inputs, resuspended sediments, isopycnal plumes, and hyperpycnal flows (Kineke et al., 2000; Mackey et al., 2002; Kuehl et al., 2004; Renagi et al., 2010; Slemons et al., 2012). These processes can transport Fe seaward across the slope (Kineke et al., 2000; Kuehl et al., 2004; Renagi et al., 2010). These lithogenic inputs, leading to very significant PFe excess compared to open ocean values, extend throughout the sampled water column (0–1000 m) at all stations in the western equatorial Pacific. Therefore, we discuss these data below as a whole, without distinguishing between different water masses or currents.

At the western equatorial Pacific stations, PFe isotopic compositions are close to the UCC reference value, supporting a predominantly lithogenic origin discussed above (Table 2 and Fig. 4). Only two samples, from stations 24 and 25, exhibit near-zero δ^{56}DFe and δ^{56}PFe values close to −0.5 ‰, likely reflecting a hydrothermal contribution, as previously suggested by Labatut et al. (2014) for station 24. Northeastern PNG is an active margin with hydrothermal activity (Auzende et al., 2000) with shallow sources able to supply EUC via the NICU (Mackey et al., 2002).

The isotopic difference between dissolved and particulate Fe, $\Delta^{56}Fe_{DFe-PFe}$, is shown in Fig. 7. Except for one data point at the surface this difference is consistently positive, i.e., DFe is systematically heavier than PFe. This is true for 26 out of 27 data points, including the two data points discussed above with significantly different δ^{56}PFe values (attributed to hydrothermal influence). On average this difference is $\Delta^{56}Fe_{DFe-PFe} = +0.27 \pm 0.32$ ‰ (2 SD, $n = 27$). This systematic difference suggests a mechanistic link between particulate and dissolved Fe pools, associated with an isotopic fractionation. A kinetic isotopic fractionation associated with an unidirectional reaction would lead to a reaction product isotopically lighter than the reactant. In such a hypothesis, PFe being lighter than DFe, this would imply that PFe is produced from DFe (for instance by precipitation). This is totally unlikely given the predominance of lithogenic PFe sources in this area. We therefore exclude the hypothesis of a kinetic fractionation and conclude that there is an equilibrium isotopic fractionation between PFe and DFe. Equilibrium fractionation implies co-occurrence of chemical fluxes from both phases toward the other. In addition, because DFe is heavier than PFe, the processes responsible for the flux from the particulate to the dissolved phase cannot be associated with an Fe reduction process (that would produce lighter DFe, Criss, 1999). This is consistent with the oxygenated water column in this region (Table 2). The PFe to DFe flux is therefore a non-reductive release of dissolved Fe, a process named non-reductive dissolution, NRD, by Radic et al. (2011). The term NRD can refer to dissolution, as well as to other type of processes from the particulate to the dissolved phase, such as desorption. This non-reductive release of dissolved Fe probably reflects processes similar to the reversible scavenging process proposed for Th or rare earth elements (REE) (Bacon and Anderson, 1982; Nozaki et al., 1987; Nozaki and Alibo, 2003). These conclusions have been

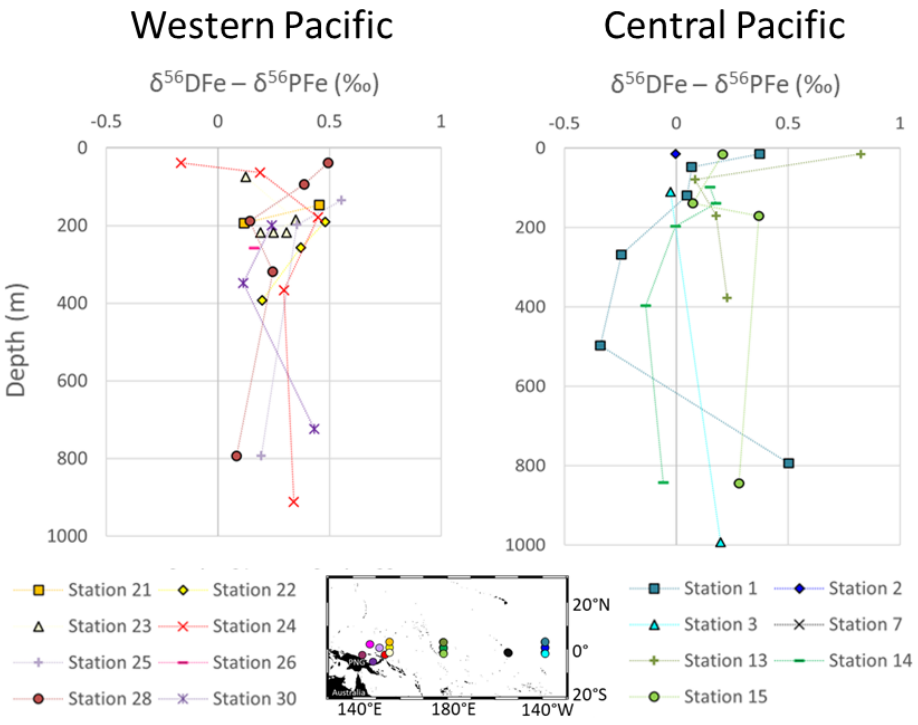

Figure 7. Differences between the dissolved and particulate of iron isotopic compositions (δ^{56}DFe – δ^{56}PFe) from the surface to 1000 m depth in the western equatorial and central equatorial Pacific.

previously proposed for stations 24, 28 and 30 (Radic et al., 2011; Labatut et al., 2014). The addition of data from five additional western stations reinforces the conclusions drawn from earlier studies and extends the geographic scope of these findings eastward beyond the Bismarck Sea, to as far as 156° E. This confirms the significant role of lithogenic inputs from PNG on the biogeochemistry of the area. These processes govern particulate – dissolved interactions at least up to 1200 km from the source, within the upper 1000 m of the water column.

The non-reductive release of dissolved iron, NRD, at the sediment/water column interface has now been observed in numerous studies as a significant external DFe source. These include the western Pacific (Radic et al., 2011; Labatut et al., 2014; this study), the northwest Atlantic (Conway and John, 2014), the northeast Atlantic (Klar et al., 2018), the southeast Atlantic (Conway et al., 2016), the Southern Ocean (Abadie et al., 2017; Tian et al., 2023) and in the southeast Pacific (John et al., 2018). In the water column, exchange fluxes between particulate and dissolved phases, including non-reductive release of dissolved iron from the particles, have also been proposed in several other studies (Radic et al., 2011; Abadie et al., 2017; Fitzsimmons et al., 2017; John et al., 2018). In all cases, at the sediment/seawater interface and within the water column, the exact processes involved remain unclear. Desorption and ligand-promoted dissolution have been suggested (Abadie et al., 2017; John et al., 2018; Homoky et al., 2021). Additionally, direct comparison of DFe and total PFe isotopic compositions has inherent limitations, as it does not allow us to study the distinct processes related to different PFe phases (lithogenic, biogenic, Fe oxyhydroxides). Those PFe phases are likely not equally involved in particulate – dissolved exchanges. Nevertheless, our analytical approach employs total digestion to guarantee the absence of artifactual isotopic fractionation. The regional geochemical characteristics establish that excess PFe is predominantly lithogenic (Fig. 6), with excess DFe correspondingly derived from this source. Although lithogenic iron is conventionally considered refractory, neodymium isotope studies have shown that lithogenic phases do dissolve, even if in small proportions (Lacan and Jeandel, 2005; Rousseau et al., 2015). The excess DFe in the area, from 0.30 to 0.63 nmol kg^{-1}, affects 19.4 Sv (Germineaud et al., 2016). This leads to a required flux of $\sim$ 540 g(DFe) s^{-1}. The riverine PFe discharge to this area is about 1.2×10^{11} g(PFe) d^{-1}. Therefore, the dissolution of only 0.04 % of the PFe discharge would be sufficient to account for the observed DFe increase. This very low dissolution rate makes it entirely plausible that the excess DFe originates from the dissolution of lithogenic PFe.

5.2 Iron sources and biogeochemical dynamics in the central equatorial Pacific

In the central equatorial Pacific, the data are discussed within each of the five density layers defined in Sect. 2 in order to

take into account different water masses and dominant currents. Western stations are included in the figures solely to illustrate potential sources to this central Pacific area. To facilitate interpretation, the δ^{56}Fe color scales are different for each density layer.

5.2.1 Surface layer, the chlorophyll maximum layer (< 120 m; < 23.8 kg m^{-3})

Having both dissolved and particulate iron data in the open ocean surface layer, far from continental inputs, provides an opportunity to quantify isotopic fractionation associated with biological uptake, i.e., consumption of dissolved Fe by phytoplankton and its consequent transfer to the particulate pool. We focus on the chlorophyll maximum layer (found between 10 and 100 m, based on fluorescence data shown in Fig. A2), also called the deep chlorophyll maximum (DCM), where the phytoplanktonic contribution to sampled particles is likely to be large. During the EUCFe cruise, the phytoplankton community was studied at station 2 at a depth of 10 m (Marchetti et al., 2010), and in the chlorophyll maximum layer at station 2, station 25, and at two other stations lacking iron isotope measurements (0, 165° E and 0, 170° W) (Johnson et al., 2010). The cyanobacteria *Prochlorococcus* and *Synechococcus* dominate this community, followed by small pennate diatoms such as *C. closterium* and *N. bicapitata* (Johnson et al., 2010; Marchetti et al., 2010). This observation is consistent with previous studies in this equatorial upwelling region, which report a predominantly cyanobacteria-based community (Chavez et al., 1990; Landry et al., 1996). Unicellular diazotrophic cyanobacteria were also identified throughout the cruise, primarily picocyanobacteria, while the larger *Trichodesmium* was found only in coastal waters (Bonnet et al., 2009).

PFe can be composed of lithogenic, biogenic, and chemogenic fractions. Chemogenic particles are formed by chemical reactions such as Fe oxyhydroxide precipitations and are frequently referred to as "authigenic". However, this term lacks precision as it merely designates material formed in situ, which could theoretically include biogenic fractions. Assuming Aluminum (Al) is entirely lithogenic (Murray et al., 1993; Frank et al., 1995; McManus et al., 1999; Cardinal et al., 2001; Dammshäuser, 2012), the lithogenic fraction of the particulate iron, $[\mathrm{PFe}]_{\mathrm{lithogenic}}$, is estimated by:

$$[\mathrm{PFe}]_{\mathrm{lithogenic}} = [\mathrm{PAl}]_{\mathrm{measured}} \times \left(\frac{[\mathrm{PFe}]}{[\mathrm{PAl}]}\right)_{\text{reference material}} \quad (3)$$

where $[\mathrm{PAl}]_{\mathrm{measured}}$ is the measured particulate Al concentration and $[\mathrm{PFe}]/[\mathrm{PAl}]_{\text{reference material}}$ is the ratio in a reference lithogenic material. Surface currents in our studied area are mainly eastward in the western Pacific and westward in the central Pacific. We therefore looked for reference lithogenic material on both the western and eastern boundaries of the Pacific basin. The Fe/Al ratios of igneous rocks from Papua New Guinea (Tiangang et al., 2024) and of igneous rocks from the Galapagos Islands and the southwestern Andes basins of Peru (Wilson et al., 2022; Ccanccapa-Cartagena et al., 2023) are equal to 0.502 mol mol^{-1} and 0.499 mol mol^{-1} respectively. Given the similarity of these ratios, we utilized an average value of 0.50 mol mol^{-1} for all samples.

In the chlorophyll maximum layer, we found that an average of 42 % mol mol^{-1} of particulate iron (PFe) is lithogenic (Table A3). The remaining 58 % mol mol^{-1} can be attributed to biogenic and chemogenic sources. The chemogenic fraction cannot be distinguished and quantified in the present study (this would have required, for example, direct measurements of phytoplankton stoichiometry and phosphorus), and there is no known isotopic signature specific to this chemogenic fraction in the literature (which is essential for Eq. 4). Because we are looking at samples taken in the chlorophyll maximum, we will assume in the following that the chemogenic Fe is negligible. This assumption is supported by observations reporting minimum chemogenic contribution in the chlorophyll maximum layer (Sofen et al., 2023) and modelling work estimating that the biogenic fraction dominates in the central equatorial Pacific (Tagliabue et al., 2023). We also assume that biogenic Fe is entirely phytoplanktonic Fe ($\mathrm{PFe}_{\mathrm{Phyto}}$) and assuming mass conservation, $\delta^{56}\mathrm{PFe}_{\mathrm{Phyto}}$ can be estimated from:

$$[\mathrm{PFe}]_{\mathrm{Phyto}}\delta^{56}\mathrm{PFe}_{\mathrm{Phyto}} \approx [\mathrm{PFe}]\delta^{56}\mathrm{PFe} - [\mathrm{PFe}]_{\mathrm{lithogenic}}\ \delta^{56}\mathrm{PFe}_{\mathrm{lithogenic}} \quad (4)$$

where [PFe] and δ^{56}PFe are the measured particulate Fe concentration and isotopic composition. The lithogenic PFe is assumed to be characterized by average crustal signature $\delta^{56}\mathrm{PFe}_{\mathrm{lithogenic}} = +0.07 \pm 0.02$ ‰ (Poitrasson, 2006). The estimated isotope compositions of phytoplanktonic PFe are shown in Fig. 8 and Table A3. $\delta^{56}\mathrm{PFe}_{\mathrm{Phyto}}$ varies from $+0.30 \pm 0.12$ ‰ to $+0.73 \pm 0.17$ ‰. Propagation of uncertainties for Fe and Al concentrations and Fe isotopes in both the samples and the reference material implies uncertainties for $\delta^{56}\mathrm{PFe}_{\mathrm{Phyto}}$ significantly higher than those of our initial data.

At three stations, the isotope data are available for both the dissolved and the phytoplanktonic iron. This allows an estimate of isotope fractionation associated with phytoplankton uptake. Assuming two simple isotopic models, either an equilibrium fractionation model (implying bidirectional chemical reactions) or a kinetic fractionation model in which phytoplankton is the instantaneous product of DFe (implying unidirectional chemical reactions), the isotopic fractionation can be calculated, with the same simple equation (Hayes, 2004):

$$\Delta^{56}\mathrm{Fe}_{\text{Phyto-DFe}} = \delta^{56}\mathrm{PFe}_{\mathrm{Phyto}} - \delta^{56}\mathrm{DFe} \quad (5)$$

This leads to $\Delta^{56}\mathrm{Fe}_{\text{Phyto-DFe}} = +0.22 \pm 0.21$ ‰ at station 1, -0.05 ± 0.14 ‰ at station 13 and $+0.15 \pm 0.19$ ‰ at station 14, with a grand average value of $\Delta^{56}\mathrm{Fe}_{\text{Phyto-DFe}} =$

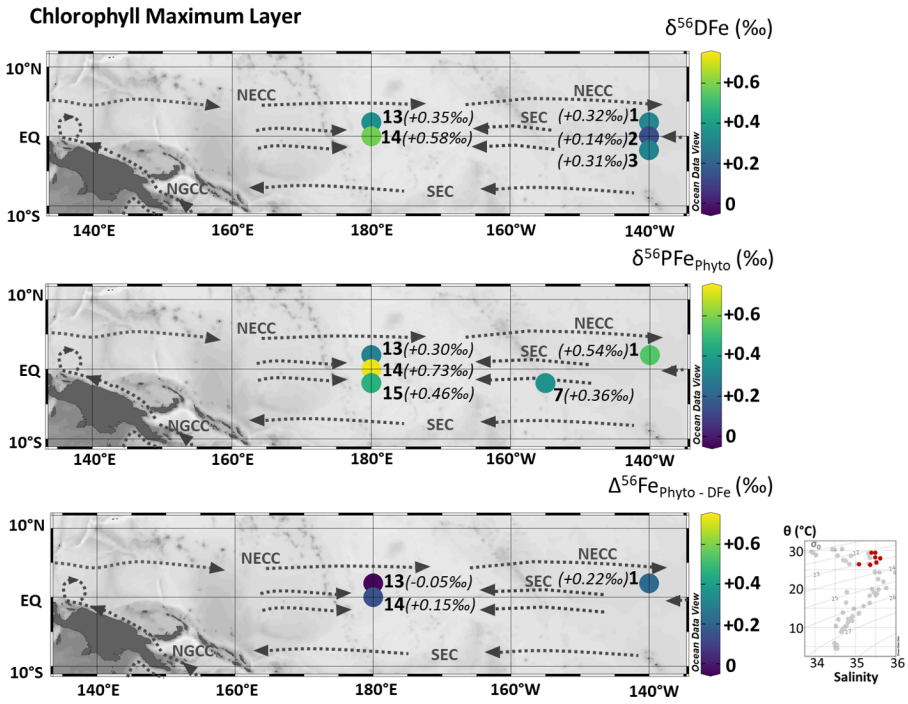

Figure 8. From the top to bottom, samples collected in the chlorophyll maximum layer, maps of δ^{56}DFe (‰), δ^{56}PFe$_{\text{Phyto}}$ (‰), and the difference between δ^{56}PFe$_{\text{Phyto}}$ and δ^{56}DFe. Station numbers are displayed next to the colored dots on the map. Main currents are represented: South Equatorial Current (SEC), North Equatorial CounterCurrent (NECC) and New Guinea Coastal Current (NGCC). In the bottom right corner, potential temperature (θ, °C) and salinity (S) of EUCFe samples. Samples in this chlorophyll maximum layer are shown in red. Values are shown in parentheses due to the large range, which limits color scale readability. Their measurement uncertainties can be found in Sect. 5.2.1 and Table 2. This figure was produced using Ocean Data View (Schlitzer, 2025).

$+0.11 \pm 0.28$ ‰ (2 SD, $n = 3$) (Fig. 8 and Table A3). Given the uncertainties, we cannot conclude that there is isotopic fractionation associated with biological uptake, but our data indicate that if it exists, it is small and lies between -0.17 ‰ and $+0.39$ ‰ ($+0.11 \pm 0.28$) at a 95 % confidence level.

These results can be compared with previous studies. Some suggest preferential uptake of light and others of heavy isotopes. From the same cruise, Radic et al. (2011) found Δ^{56}Fe$_{\text{Phyto-DFe}} = -0.25 \pm 0.10$ ‰ (2 SD) with one model and -0.13 ± 0.11 ‰ (2 SD) with a second model. While the first model was based solely on DFe data, the second incorporated PFe data assuming PFe was exclusively phytoplanktonic, whereas our results indicate a substantial lithogenic contribution at the open ocean stations (Table A3). Additional data and novel methodological approaches have refined these estimates. Off New Zealand, during the annual spring bloom, Ellwood et al. (2015) estimated an isotopic fractionation of -0.54 ‰. In that study the isotopic signatures of the particles were used, but not corrected for their lithogenic fractions, despite proximity to the mainland, and fractionation uncertainties were not discussed. In two Antarctic coastal polynyas, preferential uptake of light isotopes was suggested based on water mass DFe signatures alone (without PFe data), with isotopic fractionation of -1 ‰ ($\alpha = \delta^{56}\text{Fe}_{\text{Biomass}}/\delta^{56}\text{Fe}_{\text{Seawater}} = 0.999$) (Sieber et al., 2021) and of -1.8 ‰ to -1 ‰ ($\alpha = 0.9982$ to 0.9990) (Tian et al., 2023). However, both studies highlighted the co-occurrence of multiple mechanisms and, therefore, of several isotopic fractionation processes in the surface layer. Ellwood et al. (2020) conducted a study using both DFe and PFe isotope data in a 1-D model, and found isotopic fractionation values for biological uptake ranging from -1 ‰ (in a simplified model considering only biological uptake) to -0.6 ‰ when using a more sophisticated model representing additional processes (regeneration, scavenging and complexation) in a cold-core eddy in the Southern Ocean. Again, fractionation uncertainties were not discussed in these three studies. Finally, in the North Atlantic, two studies suggested a positive fractionation (contrasting with the previous studies) based on water mass DFe signatures (no PFe data) and without quantification (Conway and John, 2014; Klar et al., 2018). Culture experiments examining isotopic fractionation by several diatom and a coccolithophore species (not the dominant species in our samples; Johnson et al., 2010; Marchetti et al., 2010) revealed "no clear relationship to species, growth rate, or Fe concentration" for biological uptake, possibly due to the sensitivity of kinetic isotope effects (John et al., 2024). During these experiments, biological

uptake induced smaller fractionation (−1.3 ‰ to +0.60 ‰, mean +0.20 ± 0.38 ‰, 1 SD, $n = 62$) compared to abiotic processes (approximately −4 ‰ to +5 ‰). These laboratory observations align with our in situ observations, although a comparison is not straightforward because iron acquisition processes are very different in cyanobacteria (Sutak et al., 2020). These authors suggested that seawater δ^{56}Fe may not be greatly impacted by biological uptake (John et al., 2024); a conclusion consistent with the findings of Lacan et al. (2008), Radic et al. (2011) and this study.

The differences in biological fractionation probably reflect variations in phytoplankton community composition, ligand types (John et al., 2024), regional variability, and methodological approaches such as the direct measurement of particles and the consideration of their phases. Potential iron fractionation during biological uptake, if it occurs, may depend on numerous parameters, including species-specific iron acquisition processes (Sutak et al., 2020), as well as pH, ligand, and reductant types, which strongly influence kinetic isotope effects (John et al., 2024). Our study region is particularly challenging in this regard, as it is a cyanobacteria-dominated system where isotopic fractionation processes remain poorly understood (Mulholland et al., 2015; Swanner et al., 2017). Iron isotope fractionation by diazotrophic cyanobacteria has not been investigated, despite these organisms contributing disproportionately to Fe uptake relative to their numerical abundance (Lory et al., 2022). The present analysis does not allow us to draw conclusions regarding a preferential uptake of heavy or light iron isotopes during biological uptake. However, our results confirm that this fractionation is small, likely not larger than a few tenths of a per mil. They align with a previous study, in the Southern Ocean, where fractionation had a small amplitude, $|\Delta^{56}Fe_{Phyto\text{-}DFe}| < 0.32$ ‰, with no conclusion about the direction (Lacan et al., 2008), and culture experiments (John et al., 2024). Our analysis emphasizes the importance of taking into account error propagations and lithogenic contributions to the particulate phases, in the chlorophyll maximum in the open ocean.

5.2.2 Subsurface layer (110–220 m; 23.8–25.6 kg m^{-3}), upper EUC

The subsurface layer is composed of three water masses: the South Pacific Tropical Water (SPTW) (stations 3 and 15), the South Pacific Equatorial Water (SPEW) (stations 2, 14, 21, 22, 23, 24, 25, 28 and 30) and the North Pacific Equatorial Water (NPEW) (stations 1 and 26) (Fig. 9). At the equator, seawater within SPEW is subject to substantial renewal as it flows eastward from the western Pacific (140° E) to the central equatorial Pacific (140° W) (Tsuchiya et al., 1989; Grenier et al., 2011). This renewal is largely driven by equatorial upwelling which creates divergence in subsurface waters and subsequently generates meridional currents from both the northern and southern subtropical gyres toward the equator. These gyres ventilate the upper Equatorial Undercurrent (U-EUC), contributing approximately 9 Sv of the total 28 Sv contribution at 140° W, accounting for nearly one third of the upper EUC flow (Grenier et al., 2011).

We observed that δ^{56}DFe values were equal within uncertainties along the meridional transects between 2° N and 2° S (+0.40 ‰, +0.37 ‰ and +0.28 ‰ at 156° E, 180° E and 140° W, respectively) and similar consistency is observed for δ^{56}PFe (−0.03 ‰, +0.18 ‰ and +0.28 ‰ at the three same sections, Fig. 9 and Table 2). This isotopic homogeneity is consistent with the prevailing ocean circulation in the subsurface layer. Zonally, a slight decrease of δ^{56}DFe values and a slight increase of δ^{56}PFe values were observed eastward.

A comparison of DFe isotopic compositions (δ^{56}DFe) in EUCFe samples with data from the subtropical gyres provides further insight. While no data are available for the north subtropical gyre, this density layer has been documented in the south subtropical gyre along 170° W (GP19 cruise) at 10° S (Station 19) with δ^{56}DFe = +0.64 ± 0.32 ‰, and at the equator (Station 21) with δ^{56}DFe = +0.70 ± 0.35 ‰ (GEOTRACES Intermediate Data Product Group, 2025). These two datapoints are in good agreement. They may appear to be significantly different from our data (∼ 0.37 ± 0.1 ‰ at 180° E), however given their uncertainties, they are in reasonable agreement. They do not help explain the slight eastward decrease of δ^{56}DFe along the equator described above.

Overall, despites small variations, these observations suggest a relatively wide isotopic homogeneity at subsurface depths (110–220 m) likely driven by equatorial upwelling and the subsequent meridional transport of seawater.

5.2.3 Lower part of EUC: Central Waters (170–320 m; 25.6–26.55 kg m^{-3})

The density layer between 25.6 and 26.55 kg m^{-3} is composed of two water masses: the Western South Pacific Central Water (WSPCW) (stations 1, 2, 3, 14, 15, 22, 23, 25, 28) and the North Pacific Central Water (NPCW) (stations 13, 21, 26) (Fig. 2). WSPCW is characterized by a salinity maximum of central waters while NPCW represents a salinity minimum. The lower part of the EUC (L-EUC) is located in this density layer (Fig. 10). This current is of particular importance, since it is the major vector for Fe transport along the equator from the western to the eastern Pacific. The lower EUC is not significantly influenced by the equatorial upwelling in the western equatorial Pacific, and water mostly originates from the PNG region (Grenier et al., 2011).

Along the equator, at stations 25, 22, 14 and 2, samples have similar DFe isotopic composition (around +0.36 ‰), highlighting the lack of significant additional Fe sources to the lower EUC (Tsuchiya et al., 1989; Radic et al., 2011). δ^{56}DFe values are equal within uncertainties (Fig. 10 and Table 2). This suggests that the δ^{56}DFe signature is maintained over long distances within the EUC, a pattern previously reported by Radic et al. (2011) at two stations, and here confirmed as far east as 140° W. In contrast, δ^{56}PFe cannot be

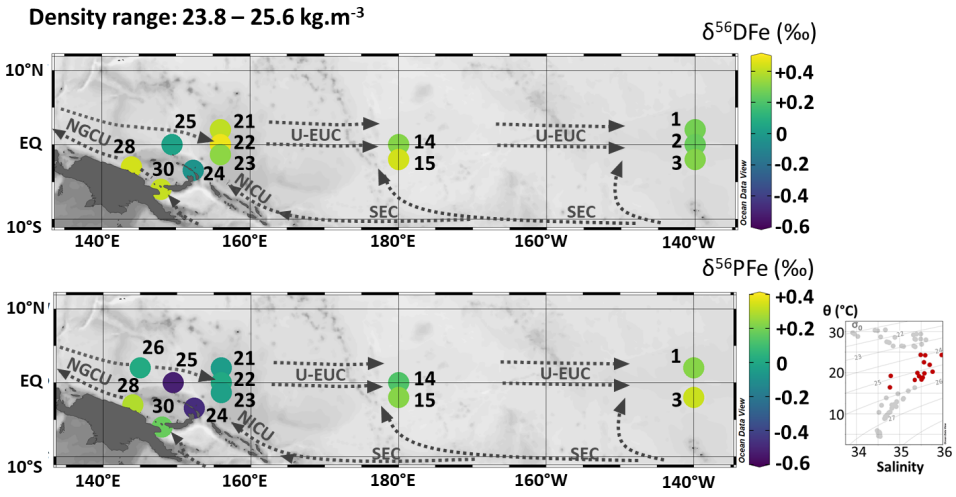

Figure 9. Map of dissolved (δ^{56}DFe) and particulate (δ^{56}PFe) iron isotopes for samples with potential densities between 23.8 and 25.6 kg m^{-3}. Station numbers are displayed next to the colored dots. Main currents are represented: the upper Equatorial Undercurrent (U-EUC), the South Equatorial Current (SEC), the New Guinea Coastal Undercurrent (NGCU) and the New Ireland Coastal Undercurrent (NICU). In the bottom right corner, potential temperature (θ, °C) and salinity (S) of EUCFe samples. Samples in this density layer are shown in red. This figure was produced using Ocean Data View (Schlitzer, 2025).

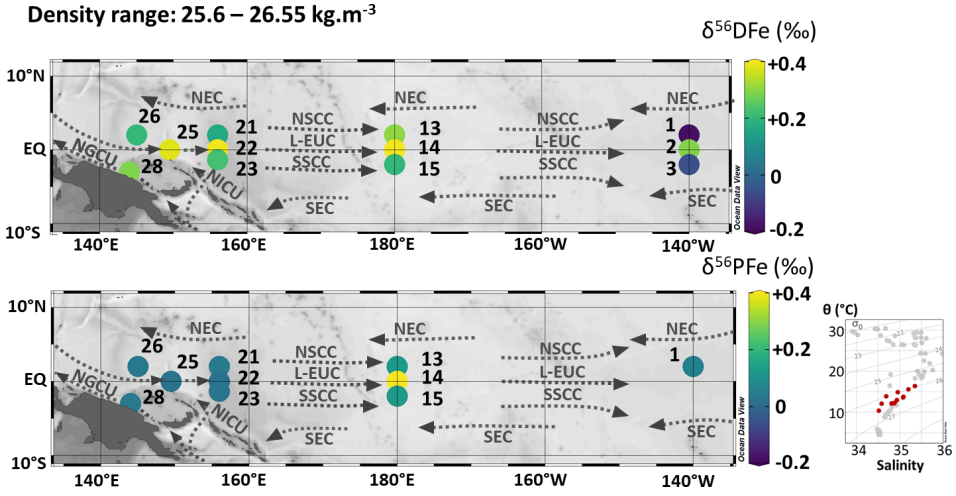

Figure 10. Map of dissolved (δ^{56}DFe) and particulate (δ^{56}PFe) iron isotopes for samples with potential densities between 25.6 and 26.55 kg m^{-3}. Station numbers are displayed next to the colored dots. Main currents are represented: the lower Equatorial Undercurrent (L-EUC), the North and South Subsurface Countercurrents (NSCC and SSCC), the North and South Equatorial Current (NEC and SEC), the New Guinea Coastal Undercurrent (NGCU) and the New Ireland Coastal Undercurrent (NICU). In the bottom right corner, potential temperature (θ, °C) and salinity (S) of EUCFe samples. Samples in this density layer are shown in red. This figure was produced using Ocean Data View (Schlitzer, 2025).

evaluated at station 2 due to missing PFe data, and values from stations 22 and 14 displayed significantly different values. These findings confirm the central role of the EUC for DFe transport across the Pacific. While earlier studies based on Fe concentrations suggested such transport (Slemons et al., 2012), isotopic data now confirm this conclusion and the fact that dissolved iron isotopic signature may be preserved, in over more than 7800 km (from station 25 to station 2). Long distance preservation of δ^{56}DFe signature has been underlined before for deeper layers, notably in the North Pacific and eastern Pacific with Fe transport from sedimentary and hydrothermal sources (Fitzsimmons et al., 2017; John et al., 2018; Sieber et al., 2024). Such a long distance of preservation of the δ^{56}DFe signature had never been observed before.

Samples from stations 1 and 3 differ significantly from the other samples. They are characterized by negative dissolved iron isotopic compositions (−0.19 ‰ and −0.06 ‰) (Fig. 10 and Table 2). They are characterized by oxygen concentra-

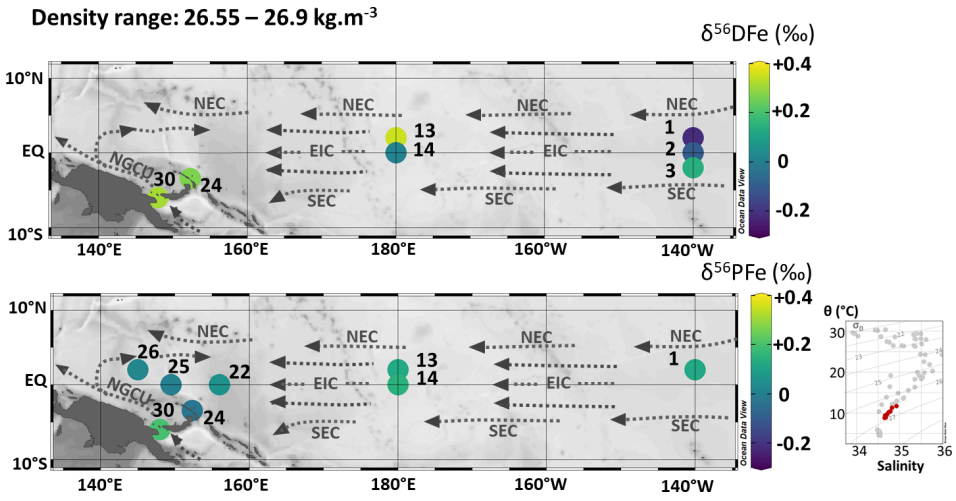

Figure 11. Map of dissolved (δ^{56}DFe) and particulate (δ^{56}PFe) iron isotopes for samples with potential densities between 26.55 and 26.9 kg m^{-3}. Station numbers are displayed next to the colored dots. Main currents are represented: the Equatorial Intermediate Current (EIC), the North and South Equatorial Current (NEC and SEC), and the New Guinea Coastal Undercurrent (NGCU). In the bottom right corner, potential temperature (θ, °C) and salinity (S) of EUCFe samples. Samples in this density layer are shown in red. This figure was produced using Ocean Data View (Schlitzer, 2025).

tions which are notably lower than those typically found in the core of the EUC (43 and 25 µmol kg^{-1}, compared to typical values around 130 µmol kg^{-1}). The currents supplying these stations, the SEC and NEC, originate from the east. These three observations support the conclusion that their Fe content may originate, at least partially, from the Californian and/or Peruvian oxygen minimum zones (OMZ). Those have been documented before, with negative or zero δ^{56}DFe values in the Californian OMZ (John et al., 2012), and DFe concentrations and isotopic compositions, around 1 nM and −0.5 ‰, observed around 12° S near the Peruvian coast (85 to 80° W) during the GP16 cruise (John et al., 2018). As above, this suggests a δ^{56}DFe signature preservation over long distances, on the order of 6400 km.

In the density layer of the lower EUC, iron isotopes reveal the presence of two distinct Fe sources in the central Pacific, lithogenic inputs from Papua New Guinea transported within the EUC, and also a likely additional eastern source from the eastern Pacific oxygen minimum zones.

5.2.4 South Antarctic Mode Water and Lower Central Waters (340–480 m; 26.55–26.9 kg m^{-3})

The density layer between 26.55 and 26.9 kg m^{-3} is composed of two water masses: the South Antarctic Mode Water (SAMW) (stations 22, 24, 25) and the Western South Pacific Central Water (WSPCW) (stations 1, 2, 3, 13, 14, 26, 30). In contrast to the shallower density layers, where currents predominantly flow eastward, this deeper layer exhibits westward currents (Fig. 11).

DFe isotopic compositions at stations 1, 2, 3, 13 and 14 were variable: negative or near zero δ^{56}DFe at stations 1, 2 and 14 (between −0.22 ‰ and +0.01 ‰) and positive δ^{56}DFe at stations 3 and 13 (+0.14 ‰ and +0.35 ‰) (Fig. 11 and Table 2). δ^{56}DFe values increased westward from station 1 (−0.22 ± 0.09 ‰) to station 13 (+0.35 ± 0.07 ‰) and from station 2 (-0.10 ± 0.07 ‰) to station 14 (+0.01 ± 0.07 ‰). This westward increase in δ^{56}DFe follows the predominant direction of zonal currents. It is consistent with data from GP19 at 170° W at the equatorial station 21 (−0.07 ± 0.05 ‰, depth of 469 m) (GEOTRACES Intermediate Data Product Group, 2025). In contrast, δ^{56}PFe values at stations 1, 13, and 14 were indistinguishable from one another and similar to the UCC reference value. Samples from stations 1, 2, 3, 13 and 14 exhibited low oxygen concentrations (< 64 µmol kg^{-1}). In contrast, samples from the western equatorial Pacific (stations 22, 24, 25, 26 and 30) had oxygen concentrations ranging from 101 to 162 µmol kg^{-1}.

These isotopic and oxygen observations suggest an Fe source from the eastern Pacific oxygen minimum zones (OMZ) and a progressive decline in the influence of eastern Pacific waters with the increase of δ^{56}DFe westward. It is consistent with our understanding of large-scale circulation patterns at these depths across the Pacific basin, and with the signatures of these areas as described above (John et al., 2012, 2018). In contrast, particulate data were indistinguishable from those of the UCC all along the EUCFe cruise and therefore do not reflect hydrodynamic structures.

5.2.5 Intermediate Waters (SEqIW and AAIW) (720–1000 m; 27.1–27.4 kg m^{-3})

The density layer between 27.1 and 27.4 kg m^{-3} is composed of two intermediate water masses: the South Equatorial Inter-

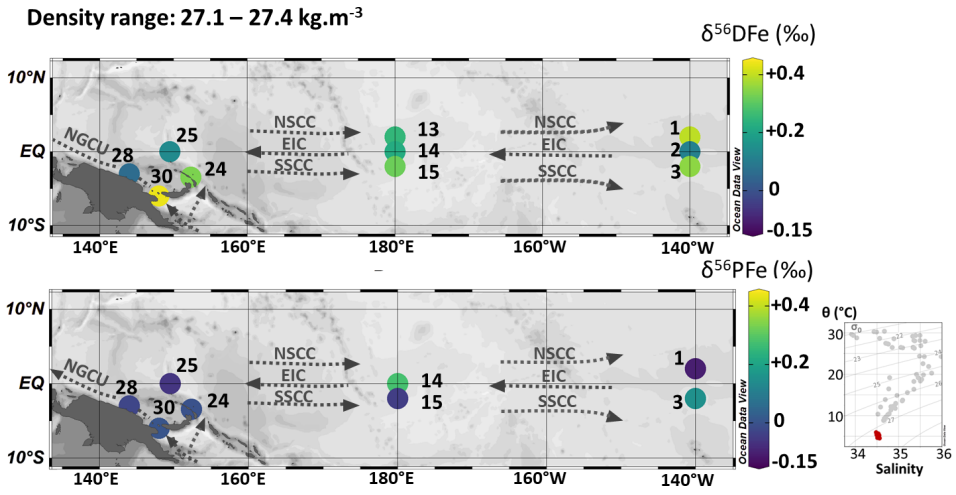

Figure 12. Map of dissolved (δ^{56}DFe) and particulate (δ^{56}PFe) iron isotopes for samples with potential densities between 27.1 and 27.4 kg m^{-3}. Station numbers are displayed next to the colored dots. Main currents are represented: the Equatorial Intermediate Current (EIC), the North and South Subsurface Countercurrents (NSCC and SSCC), and the New Guinea Coastal Undercurrent (NGCU). In the bottom right corner, potential temperature (θ, °C) and salinity (S) of EUCFe samples. Samples in this density layer are shown in red. This figure was produced using Ocean Data View (Schlitzer, 2025).

mediate Water (SeqIW) (stations 1, 2, 3, 13, 14, 15, 25) and the Antarctic Intermediate Water (AAIW) (stations 24, 28, 30) (Fig. 12). In this layer, the Equatorial Intermediate Current (EIC), a westward current, is surrounded by two eastward currents, the North and South Subsurface Countercurrents (NSCC and SSCC). The water of the EIC is sheared between the NSCC and SSCC currents at about 2° N and 2° S, causing mixing of water brought in by different currents.

Along the equator, a uniform δ^{56}DFe signature was observed between stations 2, 14 and 25, around +0.15 ‰. North and south of it, in the NSCC and the SSCC, the δ^{56}DFe signatures were significantly heavier, around +0.32 ‰ and +0.34 ‰ respectively, and did not vary significantly zonally. This is consistent with the hydrodynamic structure (westward flowing EIC at the Equator and eastward flowing NSCC and SSCC at 2° N and 2° S) and may also reflect slightly lighter signatures originating from the eastern Pacific compared to the western Pacific. In contrast, no such consistency was observed for the δ^{56}PFe values.

δ^{56}DFe of the AAIW and SeqIW from this study are compared with data from the South Pacific, GPpr11 (in the Southern Ocean, south of Australia) and GP16 cruises (John et al., 2018; Ellwood et al., 2020) in Fig. 13. The EUCFe AAIW signature (sampled at the western stations 24, 28 and 30 only) fell within the range of data previously reported, but with less variability (from +0.06 ‰ to +0.44 ‰, with an average of +0.28 ‰). As explained previously this likely reflects the impact of particulate – dissolved exchange and non-reductive dissolution processes which buffer the isotopic signature of this water mass toward about +0.3 ‰, in the PNG area.

The SEqIW (sampled at stations 1, 2, 3, 13, 14, 15, and 25) results from the mixing between the AAIW and the Pacific Deep Water (PDW). Its signatures fall within the range observed for those waters masses in previous studies, but they fall in the heavy range of those values and again have a smaller variability (from +0.11 ‰ to +0.40 ‰, average value of +0.24 ‰). This confirms (1) the large contribution of AAIW to the iron content of SEqIW and the fact that AAIW transits from the South through the PNG area and notably Vitiaz Strait before spreading in the equatorial band (Tomczak and Godfrey, 2003; Bostock et al., 2010), and (2) that the PDW contributing to the SEqIW reaches the Equatorial band with minor contribution from eastern Pacific OMZ derived iron, characterized by light isotopic signatures (John et al., 2018).

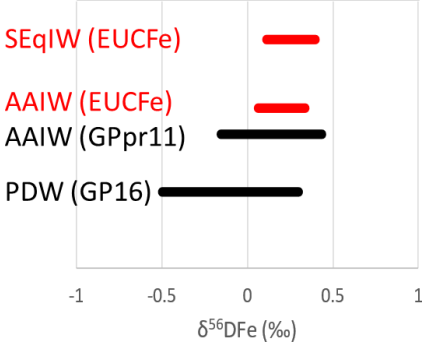

Figure 13. Comparison of δ^{56}DFe values in different water masses: the SEqIW sampled during EUCFe cruise (this study), the AAIW sampled during EUCFe (this study) and GPpr11 cruises (Ellwood et al., 2020) and the PDW sampled during GP16 cruise (John et al., 2018).

6 Conclusions

The main conclusions resulting from this study of concentrations and isotope compositions for iron in the upper 1000 m of the water column between 140° E and 140° W are shown in Fig. 14.

The goal of the EUCFe cruise was to determine the distribution of Fe along the equator between Papua New Guinea (PNG) and 140° W and to investigate the role of the Equatorial Undercurrent (EUC) in the Fe supply to the central equatorial Pacific. This study reports seawater Fe concentrations and isotopic compositions (δ^{56}Fe) in both the dissolved (DFe) and particulate (PFe) phases. By adding data from 11 additional stations, this work significantly enriches the data previously published from four stations on the same cruise (Radic et al., 2011; Labatut et al., 2014) and introduces a novel suggestion about an iron source from the eastern Pacific OMZ. The isotopic compositions ranged from -0.25 ‰ to $+0.79$ ‰ for dissolved iron and from -0.56 ‰ to $+0.48$ ‰ for particulate iron. Two distinct groups of stations were identified on the basis of Fe concentrations: western Pacific stations displaying PFe and DFe concentrations approximately seven times and twice larger than typical open ocean concentrations, respectively (stations 21, 22, 23, 24, 25, 26, 28, and 30, all located within 1200 km of the Papua New Guinea coast) and central Pacific open ocean stations, with PFe and DFe typical of the open ocean (stations 1, 2, 3, 7, 13, 14, and 15).

In the western equatorial Pacific, a large predominance of PFe concentrations over that of DFe was observed (80 % mol mol^{-1} PFe compared to total Fe, on average). The isotope signature of PFe approached that of the UCC confirming the major influence of previously documented lithogenic inputs from PNG in this area (Milliman et al., 1999; Slemons et al., 2012). At two stations, distinctly light δ^{56}DFe and δ^{56}PFe signatures suggested local hydrothermal inputs. At all stations of this western area, a systematic positive difference between δ^{56}DFe and δ^{56}PFe was observed, $\Delta^{56}Fe_{DFe-PFe} = +0.27 \pm 0.32$ ‰ (2 SD, $n = 27$). This is interpreted as the result of equilibrium isotopic fractionation, in other words the co-occurrence of chemical fluxes from both phases toward the other. This probably reflects processes similar to the reversible scavenging process proposed for Th or REE (Bacon and Anderson, 1982; Nozaki et al., 1987; Nozaki and Alibo, 2003), as previously proposed (Abadie et al., 2017). Desorption and/or ligand-promoted dissolution are potential mechanisms, though the exact processes involved remain unclear (Abadie et al., 2017; Homoky et al., 2021). Isotopic signatures suggest that Fe is primarily released via non-reductive release of dissolved Fe from suspended particles and/or oxic sediment. New data from 11 additional stations demonstrate that this process extends up to 1200 km from the Papua New Guinea coast.

In the open ocean, between 180° E and 140° W, data from the chlorophyll maximum layer were used to estimate isotopic fractionation associated with phytoplankton uptake. Our data suggest that isotopic fractionation during phytoplankton uptake is small, on the order of a few tenths of per mil. Estimates of fractionation due to biological uptake must include consideration of phytoplankton composition, dominated here by cyanobacteria. Just below this layer, within the upper EUC, δ^{56}Fe values remain homogeneous across a broad region spanning 2° N to 2° S and 156° E to 140° W, consistent with equatorial upwelling and meridional Fe inputs. In the lower EUC, a DFe isotopic signature of $\sim +0.36$ ‰, from Papua New Guinea eastward to at least 140° W, confirms the origin of the DFe carried within this current toward the HNLC area. However, an additional Fe source was identified bordering the lower EUC at 2° N and 2° S likely originating from the oxygen minimum zones (OMZ) of the eastern Pacific. This OMZ Fe source appears to be also traced deeper within central waters (200–500 m depth). The preservation of distinct Fe isotopic signatures over unprecedented long distances, 7800 km, is a key observation of this study. Finally, the limited variability of the δ^{56}DFe signatures in intermediate waters, averaging $+0.24$ ‰, confirms the major influence of AAIW transiting through the PNG area in the intermediate waters in the EUCFe area.

In conclusion, this study demonstrates the substantial influence of lithogenic inputs along ocean margins, where the water column (at least down to 1000 m) is affected by equilibrium fractionation between dissolved and particulate phases. It suggests the significance of non-reductive processes releasing dissolved iron from particulate iron. This non-reductive dissolution (NRD), occurs either at the sediment/seawater interface (i.e., external sources), or within the water column (i.e., internal processes). This highlights the need for a better understanding of these non-reductive DFe–PFe interactions, through in situ explorations, experimental work and biogeochemical modelling. Such processes likely influence the biogeochemical cycling of multiple elements. This study allowed identification of long-distance iron transport by ocean currents from an ocean margin and clarified the key role of the Equatorial Undercurrent (EUC). Finally, it suggested minor fractionation associated to phytoplankton uptake.

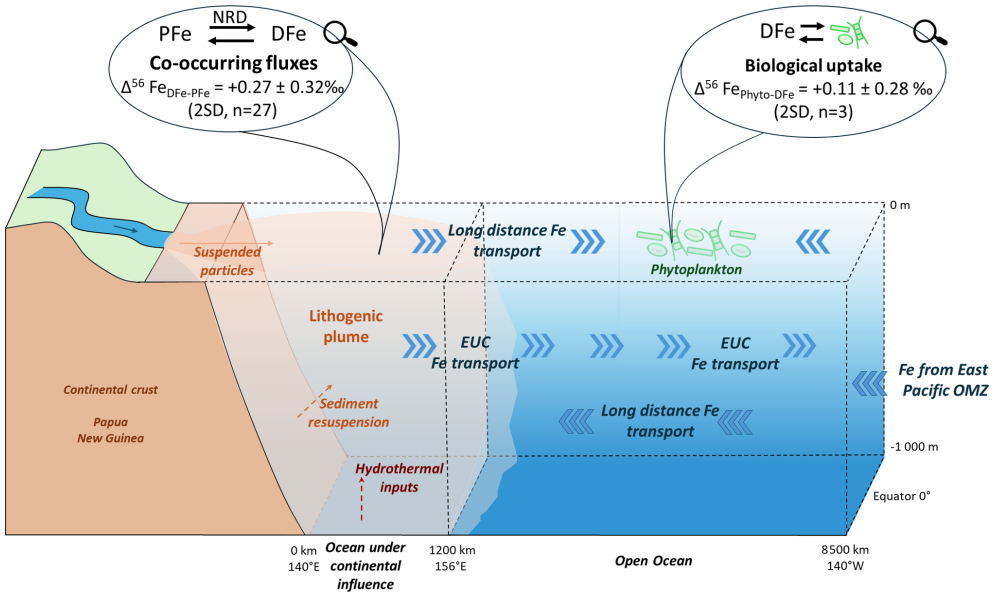

Figure 14. Illustration of Fe transport and transformation along the EUCFe cruise along the equator from the surface to 1000 m depth. OMZ stands for oxygen minimum zone and NRD for non-reductive dissolution.

Appendix A

Table A1. Sensitivity tests for different scenarios. Mean PFe concentration, Flux PFe_{SWout}, the required external sources flux, Flux $PFe_{aerosol}$ and Flux $PFe_{riverine}$ contribution to required external sources (% g g^{-1}) according to different calculation methods. Go-Flo replicates are duplicate samples taken at sea, from the same cast.

	Go-Flo bottle replicates considered separately and with the highest value (29.45 nmol kg^{-1})	Go-Flo bottle replicates considered separately and without the highest value (29.45 nmol kg^{-1})	Go-Flo bottle replicates averaged and with the highest value (29.45 nmol kg^{-1})	Go-Flo bottle replicates averaged and without the highest value (29.45 nmol kg^{-1})
Mean PFe concentration (nmol kg^{-1})	3.6 ± 4.8 (1 SD)	2.9 ± 2.3 (1 SD)	3.8 ± 5.0 (1 SD)	3.0 ± 2.5 (1 SD)
Flux PFe_{SWout} (10^6 g d^{-1})	337.9	272.2	356.7	281.6
Required external sources flux: Flux PFe_{SWout} − Flux PFe_{SWin} (10^6 g d^{-1})	323.5	257.8	342.2	267.1
Aerosol PFe flux contribution to required external sources (% g g^{-1})	82.9	104.0	78.3	100.3
Riverine PFe flux contribution to required external sources (% g g^{-1})	37 099.0	46 556.2	35 064.0	44 920.3

Table A2. Daily precipitation rates (mm d^{-1}) over the entire region considered in the box model (133° E–177° W, 9° S–15° N) from 20 to 30 September 2006. The data was obtained from Nasa Giovanni data product TRMM (3B42 Daily v7) (https://giovanni.gsfc.nasa.gov/giovanni/, last access: 30 December 2025).

Date	Precipitation Rate (TRMM 3B42 Daily v7) access in December 2025 from Nasa Giovanni data product TRMM (mm d^{-1})
20 September 2006	7.5
21 September 2006	7.7
22 September 2006	10.6
23 September 2006	8.3
24 September 2006	10.2
25 September 2006	9.0
26 September 2006	11.4
27 September 2006	13.9
28 September 2006	14.4
29 September 2006	16.5
30 September 2006	16.0
Average value	11.4 ± 6.6 (2 SD)

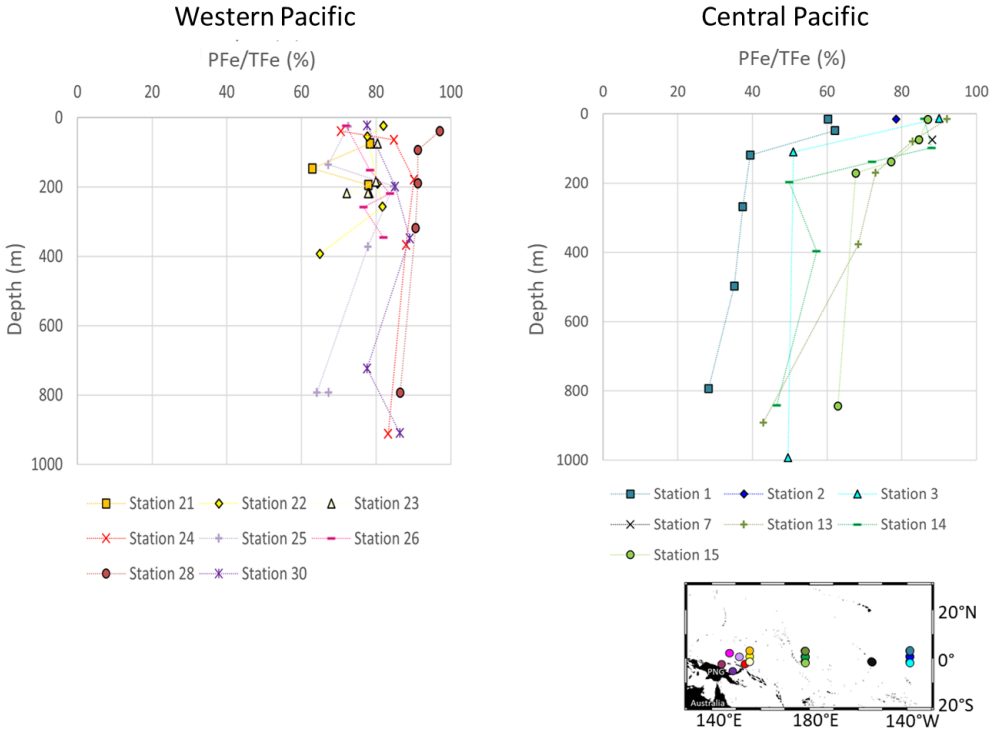

Figure A1. Fraction of particulate Fe (PFe) relative to total Fe (TFe) (% mol mol^{-1}) in the western and central equatorial Pacific.

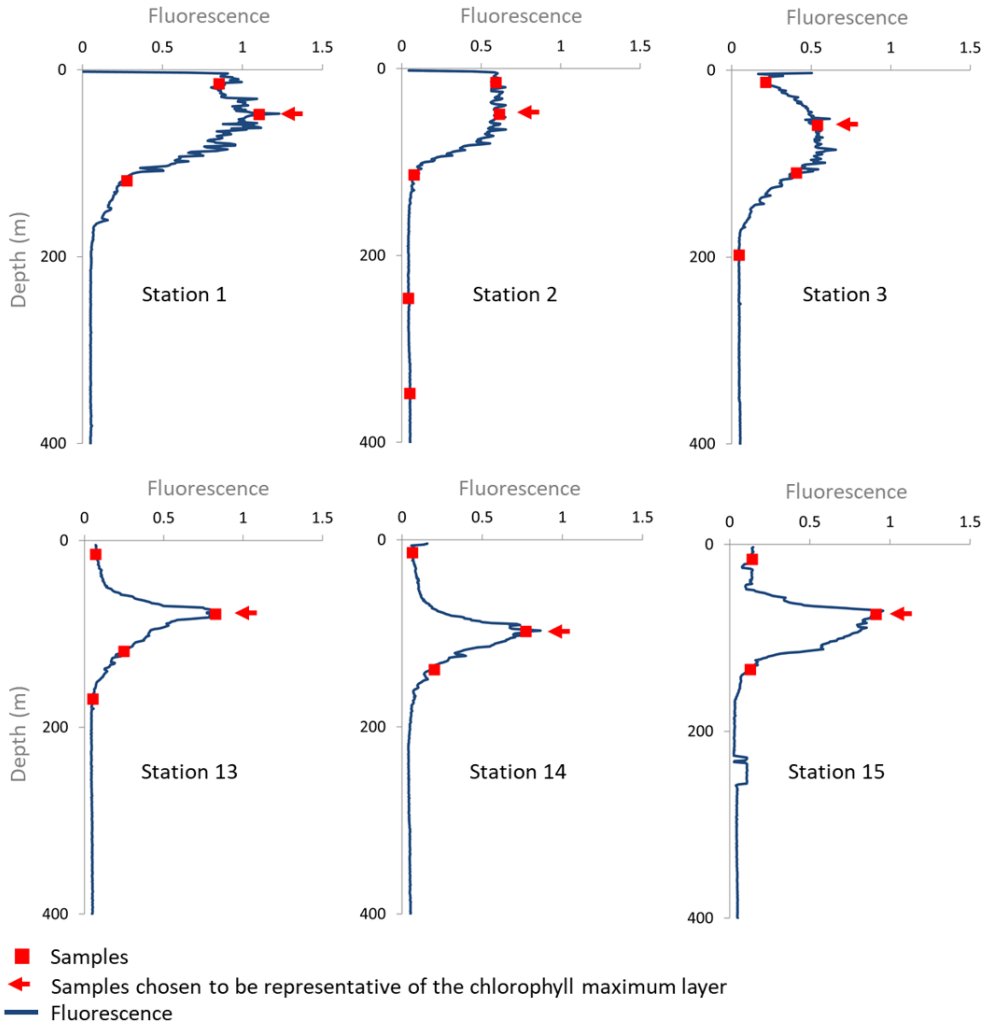

Figure A2. EUCFe cruise fluorescence profiles and sampling depth. Note that the fluorescence profiles were measured in the closest (in time) Niskin rosette cast at the same station. Samples chosen as representative of the chlorophyll maximum are shown by the (←) symbol.

Table A3. Concentrations of particulate Fe and Al, dissolved Fe isotopic composition, estimated fractions of particulate phytoplanktonic and lithogenic Fe, isotopic composition of phytoplanktonic particulate Fe and the isotopic fractionation during biological uptake ($\Delta^{56}Fe_{Phyto\text{-}DFe}$) in the chlorophyll maximum layer. Uncertainties are reported as 95 % confidence levels. Relative uncertainties for Fe and Al concentrations are 4.3 % (95 % confidence level).

Station	Depth (m)	PFe_{total} (nmol kg^{-1})	$\delta^{56}DFe$ (‰)	PAl (nmol kg^{-1})	$PFe_{lithogenic}$ (% mol mol^{-1})	PFe_{Phyto} (% mol mol^{-1})	$\delta^{56}PFe_{Phyto}$ (‰)	$\Delta^{56}Fe_{Phyto\text{-}DFe}$ (‰)
Station 1	48	0.43	$+0.32 \pm 0.07$	0.53	61.7	38.3	$+0.54 \pm 0.19$	$+0.22 \pm 0.21$
Station 2	49	–	$+0.14 \pm 0.09$	6.65	–	–	–	–
Station 3	59	–	$+0.31 \pm 0.07$	0.67	–	–	–	–
Station 7	75	0.55	–	0.53	49.0	51.0	$+0.36 \pm 0.14$	–
Station 13	79	0.49	$+0.35 \pm 0.07$	0.15	15.2	84.8	$+0.30 \pm 0.12$	-0.05 ± 0.14
Station 14	98	0.43	$+0.58 \pm 0.07$	0.39	45.2	54.8	$+0.73 \pm 0.17$	$+0.15 \pm 0.19$
Station 15	75	0.27	–	0.22	40.4	59.6	$+0.46 \pm 0.12$	–

Data availability. All the data used in this article are reported in Table 2. Fe concentration and isotope data are available in the SEANOE data repository (https://doi.org/10.17882/107774, Lacan et al., 2025) and are included in the GEOTRACES Data Product.

Author contributions. J.W.M. was the principal investigator of the EUCFe cruise. F.L. conceived the iron isotope work. M.L., C.P. and FL analyzed the samples. C.C., F.L. and M.L. wrote the article. All co-authors reviewed the manuscript.

Competing interests. The contact author has declared that none of the authors has any competing interests.

Disclaimer. Publisher's note: Copernicus Publications remains neutral with regard to jurisdictional claims made in the text, published maps, institutional affiliations, or any other geographical representation in this paper. The authors bear the ultimate responsibility for providing appropriate place names. Views expressed in the text are those of the authors and do not necessarily reflect the views of the publisher.

Acknowledgements. Amandine Radic is very much thanked for having carried out a part of the isotope work. Jérôme Chmeleff, Frédéric Candaudap, and Aurélie Marquet are thanked for their support with the ICP-MS at the *Observatoire Midi-Pyrénées*. Oguz Yigiterhan and Joseph Resing for their help around the Goflo bottles. The captain and the crew of the R/V *Kilo Moana* and especially the marine technicians Gabe Foreman, and Daniel Fitzgerald are acknowledged. Jay Cullen from University of Victoria is thanked for lending the trace-metal rosette. This study was funded by French and USA public funds. The CNRS (French National Center for Scientific Research) and the University of Toulouse (France) are thanked. The EUCFe expedition on the R/V *Kilo Moana* was supported by NSF OCE 0425721 (USA, James W. Murray). The Fe isotope project was funded by CNRS-INSU ISOFERIX project (France, François Lacan). Tim Conway and Matthias Sieber are acknowledged for their contributions to the GP15 and GP19 cruise data, and Derek Vance for his contributions to the GP19 cruise data; all were made available through the GEOTRACES Intermediate Data Product. The three anonymous reviewers are thanked for their comments, which allowed significantly improving the manuscript.

Financial support. This study was funded by French and USA public funds. The CNRS (French National Center for Scientific Research) and the University of Toulouse (France) are thanked. The EUCFe expedition on the R/V *Kilo Moana* was supported by NSF OCE 0425721 (USA). The Fe isotope project was funded par CNRS-INSU ISOFERIX project.

Review statement. This paper was edited by Elizabeth H. Shadwick and reviewed by three anonymous referees.

References

Abadie, C., Lacan, F., Radic, A., Pradoux, C., and Poitrasson, F.: Iron isotopes reveal distinct dissolved iron sources and pathways in the intermediate versus deep Southern Ocean, P. Natl. A. Sci. USA, 114, 858–863, https://doi.org/10.1073/pnas.1603107114, 2017.

Auzende, J.-M., Ishibashi, J.-I., Beaudoin, Y., Charlou, J.-L., Delteil, J., Donval, J.-P., Fouquet, Y., Ildefonse, B., Kimura, H., Nishio, Y., Radford-Knoery, J., and Ruøllan, E.: Extensive magmatic and hydrothermal activity documented in Manus Basin, Eos, Transactions American Geophysical Union, 81, 449–453, https://doi.org/10.1029/00EO00331, 2000.

Bacon, M. P. and Anderson, R. F.: Distribution of thorium isotopes between dissolved and particulate forms in the deep sea, J. Geophys. Res.-Oceans, 87, 2045–2056, https://doi.org/10.1029/JC087iC03p02045, 1982.

Baldacchino, G.: Islands, archipelagos and water: Insights from New Guinea, MGRSD, 29, 5–10, https://doi.org/10.2478/mgrsd-2023-0050, 2024.

Bennett, S. A., Rouxel, O., Schmidt, K., Garbe-Schönberg, D., Statham, P. J., and German, C. R.: Iron isotope fractionation in a buoyant hydrothermal plume, 5° S Mid-Atlantic Ridge, Geochim. Cosmochim. Ac., 73, 5619–5634, https://doi.org/10.1016/j.gca.2009.06.027, 2009.

Bergquist, B. A. and Boyle, E. A.: Iron isotopes in the Amazon River system: Weathering and transport signatures, Earth Planet Sc. Lett., 248, 54–68, https://doi.org/10.1016/j.epsl.2006.05.004, 2006.

Bingham, F. M. and Lukas, R.: The distribution of intermediate water in the western equatorial Pacific during January–February 1986, Deep-Sea Res. Pt. I, 42, 1545–1573, https://doi.org/10.1016/0967-0637(95)00064-D, 1995.

Bonnet, S., Biegala, I. C., Dutrieux, P., Slemons, L. O., and Capone, D. G.: Nitrogen fixation in the western equatorial Pacific: Rates, diazotrophic cyanobacterial size class distribution, and biogeochemical significance, Global Biogeochemical Cycles, 23, https://doi.org/10.1029/2008GB003439, 2009.

Bostock, H. C., Opdyke, B. N., and Williams, M. J. M.: Characterising the intermediate depth waters of the Pacific Ocean using $\delta^{13}C$ and other geochemical tracers, Deep-Sea Res. Pt. I, 57, 847–859, https://doi.org/10.1016/j.dsr.2010.04.005, 2010.

Boyle, E. A., John, S., Abouchami, W., Adkins, J. F., Echegoyen-Sanz, Y., Ellwood, M., Flegal, A. R., Fornace, K., Gallon, C., Galer, S., Gault-Ringold, M., Lacan, F., Radic, A., Rehkamper, M., Rouxel, O., Sohrin, Y., Stirling, C., Thompson, C., Vance, D., Xue, Z., and Zhao, Y.: GEOTRACES IC1 (BATS) contamination-prone trace element isotopes Cd, Fe, Pb, Zn, Cu, and Mo intercalibration, Limno. Oceanogr.-Meth, 10, 653–665, https://doi.org/10.4319/lom.2012.10.653, 2012.

Butt, J. and Lindstrom, E.: Currents off the east coast of New Ireland, Papua New Guinea, and their relevance to regional undercurrents in the western equatorial Pacific Ocean, J. Geophys. Res.-Oceans, 99, 12503–12514, https://doi.org/10.1029/94JC00399, 1994.

Camin, C., Lacan, F., Pradoux, C., Labatut, M., Johansen, A., and Murray, J. W.: Iron isotopes suggest significant aerosol dissolution over the Pacific Ocean, Atmos. Chem. Phys., 25, 8213–8228, https://doi.org/10.5194/acp-25-8213-2025, 2025.

Cardinal, D., Dehairs, F., Cattaldo, T., and André, L.: Geochemistry of suspended particles in the Subantarctic and Polar Frontal zones south of Australia: Constraints on export and advection processes, J. Geophys. Res.-Oceans, 106, 31637–31656, https://doi.org/10.1029/2000JC000251, 2001.

Ccanccapa-Cartagena, A., Chavez-Gonzales, F. D., Paredes, B., Vera, C., Gutierrez, G., Valencia, R., Lucia Paz Alcázar, A., Zyaykina, N. N., Filley, T. R., and Jafvert, C. T.: Seasonal differences in trace metal concentrations in the major rivers of the hyper-arid southwestern Andes basins of Peru, J. Environ. Manage., 344, 118493, https://doi.org/10.1016/j.jenvman.2023.118493, 2023.

Chavez, F. P., Buck, K. R., and Barber, R. T.: Phytoplankton taxa in relation to primary production in the equatorial Pacific, Deep Sea Research Part A. Oceanographic Research Papers, 37, 1733–1752, https://doi.org/10.1016/0198-0149(90)90074-6, 1990.

Chisholm, S. W. and Morel, F. M. M.: What controls phytoplankton production in nutrient-rich areas of the open sea?, in: Limnology and Oceanography, American Society of Limnology and Oceanography Symposium, San-Marcos, California, U1507–U1511, https://www.osti.gov/servlets/purl/10111942 (last access: 30 December 2025), 1991.

Coale, K. H., Fitzwater, S. E., Gordon, R. M., Johnson, K. S., and Barber, R. T.: Control of community growth and export production by upwelled iron in the equatorial Pacific Ocean, Nature, 379, 621–624, https://doi.org/10.1038/379621a0, 1996.

Cohen, N. R., Noble, A. E., Moran, D. M., McIlvin, M. R., Goepfert, T. J., Hawco, N. J., German, C. R., Horner, T. J., Lamborg, C. H., McCrow, J. P., Allen, A. E., and Saito, M. A.: Hydrothermal trace metal release and microbial metabolism in the northeastern Lau Basin of the South Pacific Ocean, Biogeosciences, 18, 5397–5422, https://doi.org/10.5194/bg-18-5397-2021, 2021.

Conway, T. M. and John, S. G.: Quantification of dissolved iron sources to the North Atlantic Ocean, Nature, 511, 212–215, https://doi.org/10.1038/nature13482, 2014.

Conway, T. M., John, S. G., and Lacan, F.: Intercomparison of dissolved iron isotope profiles from reoccupation of three GEOTRACES stations in the Atlantic Ocean, Mar. Chem., 183, 50–61, https://doi.org/10.1016/j.marchem.2016.04.007, 2016.

Cravatte, S., Kestenare, E., Marin, F., Dutrieux, P., and Firing, E.: Subthermocline and Intermediate Zonal Currents in the Tropical Pacific Ocean: Paths and Vertical Structure, J. Phys. Oceanogr., 47, 2305–2324, https://doi.org/10.1175/JPO-D-17-0043.1, 2017.

Criss, R. E.: Principles of Stable Isotope Distribution, Oxford University Press, Oxford, New York, 264 pp., ISBN 978-0-19-756119-5, 1999.

Dammshäuser, A.: Distribution and behavior of the lithogenic tracers aluminium and titanium in the upper water column of the Atlantic Ocean, Faculty of Mathematics and Natural Sciences Christian-Albrechts-Universität zu Kiel, https://nbn-resolving.org/urn:nbn:de:gbv:8-diss-81211 (last access: 16 November 2024), 2012.

Delcroix, T., Eldin, G., Radenac, M.-H., Toole, J., and Firing, E.: Variation of the western equatorial Pacific Ocean, 1986–1988, Journal of Geophysical Research: Oceans, 97, 5423–5445, https://doi.org/10.1029/92JC00127, 1992.

Ellwood, M. J., Hutchins, D. A., Lohan, M. C., Milne, A., Nasemann, P., Nodder, S. D., Sander, S. G., Strzepek, R., Wilhelm, S. W., and Boyd, P. W.: Iron stable isotopes track pelagic iron cycling during a subtropical phytoplankton bloom, P. Natl. Acad. Sci. USA, 112, E15–E20, https://doi.org/10.1073/pnas.1421576112, 2015.

Ellwood, M. J., Strzepek, R. F., Strutton, P. G., Trull, T. W., Fourquez, M., and Boyd, P. W.: Distinct iron cycling in a Southern Ocean eddy, Nat. Commun., 11, 825, https://doi.org/10.1038/s41467-020-14464-0, 2020.

Emery, W. J. and Meincke, J.: Global water masses: summary and review, Oceanol. Acta, 9, 383–391, 1986.

Fantle, M. S. and DePaolo, D. J.: Iron isotopic fractionation during continental weathering, Earth Planet Sc. Lett., 228, 547–562, https://doi.org/10.1016/j.epsl.2004.10.013, 2004.

Fiedler, P. C. and Talley, L. D.: Hydrography of the eastern tropical Pacific: A review, Prog. Oceanogr., 69, 143–180, https://doi.org/10.1016/j.pocean.2006.03.008, 2006.

Fine, R. A., Lukas, R., Bingham, F. M., Warner, M. J., and Gammon, R. H.: The western equatorial Pacific: A water mass crossroads, Journal of Geophysical Research: Oceans, 99, 25063–25080, https://doi.org/10.1029/94JC02277, 1994.

Fitzsimmons, J. N., John, S. G., Marsay, C. M., Hoffman, C. L., Nicholas, S. L., Toner, B. M., German, C. R., and Sherrell, R. M.: Iron persistence in a distal hydrothermal plume supported by dissolved–particulate exchange, Nature Geosci., 10, 195–201, https://doi.org/10.1038/ngeo2900, 2017.

Flament, P., Mattielli, N., Aimoz, L., Choël, M., Deboudt, K., Jong, J. de, Rimetz-Planchon, J., and Weis, D.: Iron isotopic fractionation in industrial emissions and urban aerosols, Chemosphere, 73, 1793–1798, https://doi.org/10.1016/j.chemosphere.2008.08.042, 2008.

Frank, M., Eisenhauer, A., Bonn, W. J., Walter, P., Grobe, H., Kubik, P. W., Dittrich-Hannen, B., and Mangini, A.: Sediment redistribution versus paleoproductivity change: Weddell Sea margin sediment stratigraphy and biogenic particle flux of the last 250,000 years deduced from 230Thex, 10Be and biogenic barium profiles, Earth Planet Sc. Lett., 136, 559–573, https://doi.org/10.1016/0012-821X(95)00161-5, 1995.

GEOTRACES Intermediate Data Product Group: The GEOTRACES Intermediate Data Product 2025 (IDP2025), NERC EDS British Oceanographic Data Centre NOC [data set], https://doi.org/10.5285/42c92148-8d03-8be6-e063-7086abc09f0c, 2025.

Germineaud, C., Ganachaud, A., Sprintall, J., Cravatte, S., Eldin, G., Alberty, M. S., and Privat, E.: Pathways and Water Mass Properties of the Thermocline and Intermediate Waters in the Solomon Sea, J. Phys. Oceanogr., 46, 3031–3049, https://doi.org/10.1175/JPO-D-16-0107.1, 2016.

Gordon, R. M., Coale, K. H., and Johnson, K. S.: Iron distributions in the equatorial Pacific: Implications for new production, Limnol. Oceanogr., 42, 419–431, https://doi.org/10.4319/lo.1997.42.3.0419, 1997.

Grenier, M.: Le rôle du pacifique tropical sud-ouest dans la fertilisation du pacifique équatorial: couplage dynamique et multitraceur, These de doctorat, Toulouse 3, 205 pp., https://theses.hal.science/tel-00876092 (last access: 4 April 2024), 2012.

Grenier, M., Cravatte, S., Blanke, B., Menkes, C., Koch-Larrouy, A., Durand, F., Melet, A., and Jeandel, C.: From the western boundary currents to the Pacific Equatorial Undercurrent: Modeled pathways and water mass evolutions, Journal of Geophysical

Research: Oceans, 116, https://doi.org/10.1029/2011JC007477, 2011.

Grenier, M., Jeandel, C., Lacan, F., Vance, D., Venchiarutti, C., Cros, A., and Cravatte, S.: From the subtropics to the central equatorial Pacific Ocean: Neodymium isotopic composition and rare earth element concentration variations, J. Geophys. Res.-Oceans, 118, 592–618, https://doi.org/10.1029/2012JC008239, 2013.

Hayes, J.: An Introduction to Isotopic Calculations, Woods Hole Oceanographic Institution, https://doi.org/10.1575/1912/27058, 2004.

He, Y., Kadko, D. C., Stephens, M. P., Sheridan, M. T., Buck, C. S., Marsay, C. M., Landing, W. M., Zheng, M., and Liu, P.: Constraining aerosol deposition over the global ocean, Nat. Geosci., 18, 966–974, https://doi.org/10.1038/s41561-025-01785-2, 2025.

Homoky, W. B., Severmann, S., Mills, R. A., Statham, P. J., and Fones, G. R.: Pore-fluid Fe isotopes reflect the extent of benthic Fe redox recycling: Evidence from continental shelf and deep-sea sediments, Geology, 37, 751–754, https://doi.org/10.1130/G25731A.1, 2009.

Homoky, W. B., Conway, T. M., John, S. G., König, D., Deng, F., Tagliabue, A., and Mills, R. A.: Iron colloids dominate sedimentary supply to the ocean interior, P. Natl. Acad. Sci. USA, 118, e2016078118, https://doi.org/10.1073/pnas.2016078118, 2021.

Ingri, J., Malinovsky, D., Rodushkin, I., Baxter, D. C., Widerlund, A., Andersson, P., Gustafsson, Ö., Forsling, W., and Öhlander, B.: Iron isotope fractionation in river colloidal matter, Earth Planet Sc. Lett., 245, 792–798, https://doi.org/10.1016/j.epsl.2006.03.031, 2006.

John, S. G., Mendez, J., Moffett, J., and Adkins, J.: The flux of iron and iron isotopes from San Pedro Basin sediments, Geochim. Cosmochim. Ac., 93, 14–29, https://doi.org/10.1016/j.gca.2012.06.003, 2012.

John, S. G., Helgoe, J., Townsend, E., Weber, T., DeVries, T., Tagliabue, A., Moore, K., Lam, P., Marsay, C. M., and Till, C.: Biogeochemical cycling of Fe and Fe stable isotopes in the Eastern Tropical South Pacific, Mar. Chem., 201, 66–76, https://doi.org/10.1016/j.marchem.2017.06.003, 2018.

John, S. G., Boyle, E. A., Cunningham, B. R., Fu, F.-X., Greene, S., Hodierne, C., Hutchins, D. A., Kavner, A., King, A. L., Rosenberg, A. D., Saito, M. A., and Wasson, A.: Kinetic Isotope Effects During Reduction of Fe(III) to Fe(II): Large Normal and Inverse Isotope Effects for Abiotic Reduction and Smaller Fractionations by Phytoplankton in Culture, Geochemistry, Geophysics, Geosystems, 25, e2023GC010952, https://doi.org/10.1029/2023GC010952, 2024.

Johnson, G. C., Sloyan, B. M., Kessler, W. S., and McTaggart, K. E.: Direct measurements of upper ocean currents and water properties across the tropical Pacific during the 1990s, Progress in Oceanography, 52, 31–61, https://doi.org/10.1016/S0079-6611(02)00021-6, 2002.

Johnson, Z., Shyam, R., Ritchie, A., Mioni, C., Lance, V., Murray, J., and Zinser, E.: The effect of iron- and light-limitation on phytoplankton communities of deep chlorophyll maxima of the western Pacific Ocean, Journal of Marine Research, 68, 283–308, https://doi.org/10.1357/002224010793721433, 2010.

Kadko, D., Landing, W. M., and Buck, C. S.: Quantifying Atmospheric Trace Element Deposition Over the Ocean on a Global Scale With Satellite Rainfall Products, Geophysical Research Letters, 47, e2019GL086357, https://doi.org/10.1029/2019GL086357, 2020.

Kashino, Y., Aoyama, M., Kawano, T., Hendiarti, N., Syaefudin, Anantasena, Y., Muneyama, K., and Watanabe, H.: The water masses between Mindanao and New Guinea, Journal of Geophysical Research: Oceans, 101, 12391–12400, https://doi.org/10.1029/95JC03797, 1996.

Kashino, Y., Ueki, I., Kuroda, Y., and Purwandani, A.: Ocean variability North of New Guinea derived from TRITON buoy data, J. Oceanogr., 63, 545–559, https://doi.org/10.1007/s10872-007-0049-y, 2007.

Kaupp, L. J., Measures, C. I., Selph, K. E., and Mackenzie, F. T.: The distribution of dissolved Fe and Al in the upper waters of the Eastern Equatorial Pacific, Deep-Sea Res. Pt. II, 58, 296–310, https://doi.org/10.1016/j.dsr2.2010.08.009, 2011.

Kineke, G. C., Woolfe, K. J., Kuehl, S. A., Milliman, J. D., Dellapenna, T. M., and Purdon, R. G.: Sediment export from the Sepik River, Papua New Guinea: evidence for a divergent sediment plume, Cont. Shelf Res., 20, 2239–2266, https://doi.org/10.1016/S0278-4343(00)00069-8, 2000.

Klar, J. K., Schlosser, C., Milton, J. A., Woodward, E. M. S., Lacan, F., Parkinson, I. J., Achterberg, E. P., and James, R. H.: Sources of dissolved iron to oxygen minimum zone waters on the Senegalese continental margin in the tropical North Atlantic Ocean: Insights from iron isotopes, Geochim. Cosmochim. Ac., 236, 60–78, https://doi.org/10.1016/j.gca.2018.02.031, 2018.

Kuehl, S. A., Brunskill, G. J., Burns, K., Fugate, D., Kniskern, T., and Meneghini, L.: Nature of sediment dispersal off the Sepik River, Papua New Guinea: preliminary sediment budget and implications for margin processes, Cont. Shelf Res., 24, 2417–2429, https://doi.org/10.1016/j.csr.2004.07.016, 2004.

Kurisu, M., Sakata, K., Miyamoto, C., Takaku, Y., Iizuka, T., and Takahashi, Y.: Variation of Iron Isotope Ratios in Anthropogenic Materials Emitted through Combustion Processes, Chem. Lett., 45, 970–972, https://doi.org/10.1246/cl.160451, 2016.

Labatut, M., Lacan, F., Pradoux, C., Chmeleff, J., Radic, A., Murray, J. W., Poitrasson, F., Johansen, A. M., and Thil, F.: Iron sources and dissolved-particulate interactions in the seawater of the Western Equatorial Pacific, iron isotope perspectives, Global Biogeochem. Cy., 28, 1044–1065, https://doi.org/10.1002/2014GB004928, 2014.

Lacan, F. and Jeandel, C.: Tracing Papua New Guinea imprint on the central Equatorial Pacific Ocean using neodymium isotopic compositions and Rare Earth Element patterns, Earth Planet Sc. Lett., 186, 497–512, https://doi.org/10.1016/S0012-821X(01)00263-1, 2001.

Lacan, F. and Jeandel, C.: Neodymium isotopes as a new tool for quantifying exchange fluxes at the continent–ocean interface, Earth and Planetary Science Letters, 232, 245–257, https://doi.org/10.1016/j.epsl.2005.01.004, 2005.

Lacan, F., Radic, A., Jeandel, C., Poitrasson, F., Sarthou, G., Pradoux, C., and Freydier, R.: Measurement of the isotopic composition of dissolved iron in the open ocean, Geophys. Res. Lett., 35, L24610, https://doi.org/10.1029/2008GL035841, 2008.

Lacan, F., Radic, A., Labatut, M., Jeandel, C., Poitrasson, F., Sarthou, G., Pradoux, C., Chmeleff, J., and Freydier, R.: High-Precision Determination of the Isotopic Composition of Dissolved Iron in Iron Depleted Seawater by Dou-

ble Spike Multicollector-ICPMS, Anal. Chem., 82, 7103–7111, https://doi.org/10.1021/ac1002504, 2010.

Lacan, F., Artigue, L., Klar, J. K., Pradoux, C., Chmeleff, J., and Freydier, R.: Interferences and Matrix Effects on Iron Isotopic Composition Measurements by 57Fe-58Fe Double-Spike Multi-Collector Inductively Coupled Plasma Mass Spectrometry; the Importance of Calcium and Aluminum Interferences, Front. Environ. Chem., 2, https://doi.org/10.3389/fenvc.2021.692025, 2021.

Lacan, F., Pradoux, C., Dutrieux, P., Murray, J. W., Johansen, A., Radic, A., and Labatut, M.: CTD, dissolved oxygen concentrations, iron concentrations and isotopic compositions in the filtered seawater, seawater suspended particles and aerosols, during the EUCFe cruise, KM0625, in the Equatorial Pacific Ocean, SEANOE [data set], https://doi.org/10.17882/107774, 2025.

Landry, M. R., Kirshtein, J., and Constantinou, J.: Abundances and distributions of picoplankton populations in the central equatorial Pacific from 12° N to 12° S, 140° W, Deep Sea Research Part II: Topical Studies in Oceanography, 43, 871–890, https://doi.org/10.1016/0967-0645(96)00018-5, 1996.

Lory, C., Van Wambeke, F., Fourquez, M., Barani, A., Guieu, C., Tilliette, C., Marie, D., Nunige, S., Berman-Frank, I., and Bonnet, S.: Assessing the contribution of diazotrophs to microbial Fe uptake using a group specific approach in the Western Tropical South Pacific Ocean, ISME Commun., 2, 41, https://doi.org/10.1038/s43705-022-00122-7, 2022.

Mackey, D. J., O'Sullivan, J. E. Os., and Watson, R. J.: Iron in the western Pacific: a riverine or hydrothermal source for iron in the Equatorial Undercurrent?, Deep-Sea Res. Pt. I, 49, 877–893, https://doi.org/10.1016/S0967-0637(01)00075-9, 2002.

Marchetti, A., Varela, D. E., Lance, V. P., Lance, V. P., Palmucci, M., Giordano, M., and Virginia Armbrust, E.: Iron and silicic acid effects on phytoplankton productivity, diversity, and chemical composition in the central equatorial Pacific Ocean, Limnology and Oceanography, 55, 11–29, https://doi.org/10.4319/lo.2010.55.1.0011, 2010.

Marsay, C. M., Lam, P. J., Heller, M. I., Lee, J.-M., and John, S. G.: Distribution and isotopic signature of ligand-leachable particulate iron along the GEOTRACES GP16 East Pacific Zonal Transect, Mar. Chem., 201, 198–211, https://doi.org/10.1016/j.marchem.2017.07.003, 2018.

Martin, J. H.: Iron as a Limiting Factor in Oceanic Productivity, in: Primary Productivity and Biogeochemical Cycles in the Sea, edited by: Falkowski, P. G., Woodhead, A. D., and Vivirito, K., Springer, Boston, MA, 123–137, https://doi.org/10.1007/978-1-4899-0762-2_8, 1992.

McCartney, M. S.: Subantarctic Mode Water, Woods Hole Oceanographic Institution Contribution 3773, 103–119, https://www.whoi.edu/science/PO/people/mmccartney/pdfs/McCartney77.pdf (last access: 15 January 2025), 1977.

McManus, J., Berelson, W. M., Hammond, D. E., and Klinkhammer, G. P.: Barium Cycling in the North Pacific: Implications for the Utility of Ba as a Paleoproductivity and Paleoalkalinity Proxy, Paleoceanography, 14, 53–61, https://doi.org/10.1029/1998PA900007, 1999.

Milliman, J. D.: Sediment discharge to the ocean from small mountainous rivers: The New Guinea example, Geo-Mar. Lett., 15, 127–133, https://doi.org/10.1007/BF01204453, 1995.

Milliman, J. D. and Syvitski, J. P. M.: Geomorphic/Tectonic Control of Sediment Discharge to the Ocean: The Importance of Small Mountainous Rivers, The Journal of Geology, 100, 525–544, https://doi.org/10.1086/629606, 1992.

Milliman, J. D., Farnsworth, K. L., and Albertin, C. S.: Flux and fate of fluvial sediments leaving large islands in the East Indies, J. Sea Res., 41, 97–107, https://doi.org/10.1016/S1385-1101(98)00040-9, 1999.

Morel, F. M. M., Lam, P. J., and Saito, M. A.: Trace Metal Substitution in Marine Phytoplankton, Annu. Rev. Earth Pl. Sc., 48, 491–517, https://doi.org/10.1146/annurev-earth-053018-060108, 2020.

Mulholland, D. S., Poitrasson, F., Shirokova, L. S., González, A. G., Pokrovsky, O. S., Boaventura, G. R., and Vieira, L. C.: Iron isotope fractionation during Fe(II) and Fe(III) adsorption on cyanobacteria, Chemical Geology, 400, 24–33, https://doi.org/10.1016/j.chemgeo.2015.01.017, 2015.

Murray, J. W., Barber, R. T., Roman, M. R., Bacon, M. P., and Feely, R. A.: Physical and Biological Controls on Carbon Cycling in the Equatorial Pacific, Science, 266, 58–65, https://doi.org/10.1126/science.266.5182.58, 1994.

Murray, R. W., Leinen, M., and Isern, A. R.: Biogenic flux of Al to sediment in the central equatorial Pacific Ocean: Evidence for increased productivity during glacial periods, Paleoceanography, 8, 651–670, https://doi.org/10.1029/93PA02195, 1993.

Nozaki, Y. and Alibo, D. S.: Dissolved rare earth elements in the Southern Ocean, southwest of Australia: Unique patterns compared to the South Atlantic data, Geochem. J., 37, 47–62, https://doi.org/10.2343/geochemj.37.47, 2003.

Nozaki, Y., Yang, H.-S., and Yamada, M.: Scavenging of thorium in the ocean, J. Geophys. Res.-Oceans, 92, 772–778, https://doi.org/10.1029/JC092iC01p00772, 1987.

Philander, S. G. H.: equatorial undercurrent: Measurements and theories, Rev. Geophys., 11, 513–570, https://doi.org/10.1029/RG011i003p00513, 1973.

Pickard, G. L. and Emery, W. J.: Descriptive Physical Oceanography, Elsevier, 348 pp., ISBN 978-0-7506-2759-7, 1990.

Poitrasson, F.: On the iron isotope homogeneity level of the continental crust, Chem. Geol., 235, 195–200, https://doi.org/10.1016/j.chemgeo.2006.06.010, 2006.

Pollard, R. T., Griffiths, M. J., Cunningham, S. A., Read, J. F., Pérez, F. F., and Ríos, A. F.: Vivaldi 1991 – A study of the formation, circulation and ventilation of Eastern North Atlantic Central Water, Prog. Oceanogr., https://doi.org/10.1016/S0079-6611(96)00008-0, 1996.

Qu, T. and Lindstrom, E. J.: A Climatological Interpretation of the Circulation in the Western South Pacific, J. Phys. Oceanogr., 32, 2492–2508, https://doi.org/10.1175/1520-0485(2002)032<2492:ACIOTC>2.0.CO;2, 2002.

Qu, T. and Lindstrom, E. J.: Northward Intrusion of Antarctic Intermediate Water in the Western Pacific, J. Phys. Oceanogr., 34, 2104–2118, https://doi.org/10.1175/1520-0485(2004)034<2104:NIOAIW>2.0.CO;2, 2004.

Qu, T., Gao, S., Fukumori, I., Fine, R. A., and Lindstrom, E. J.: Origin and Pathway of Equatorial 13 °C Water in the Pacific Identified by a Simulated Passive Tracer and Its Adjoint, J. Phys. Oceanogr., 39, 1836–1853, https://doi.org/10.1175/2009JPO4045.1, 2009.

Radic, A., Lacan, F., and Murray, J. W.: Iron isotopes in the seawater of the equatorial Pacific Ocean: New constraints for the oceanic iron cycle, Earth Planet Sc. Lett., 306, 1–10, https://doi.org/10.1016/j.epsl.2011.03.015, 2011.

Renagi, O., Ridd, P., and Stieglitz, T.: Quantifying the suspended sediment discharge to the ocean from the Markham River, Papua New Guinea, Cont. Shelf Res., 30, 1030–1041, https://doi.org/10.1016/j.csr.2010.01.015, 2010.

Rodgers, K. B., Blanke, B., Madec, G., Aumont, O., Ciais, P., and Dutay, J.-C.: Extratropical sources of Equatorial Pacific upwelling in an OGCM, Geophys. Res. Lett., 30, https://doi.org/10.1029/2002GL016003, 2003.

Rousseau, T. C. C., Sonke, J. E., Chmeleff, J., van Beek, P., Souhaut, M., Boaventura, G., Seyler, P., and Jeandel, C.: Rapid neodymium release to marine waters from lithogenic sediments in the Amazon estuary, Nat. Commun., 6, 7592, https://doi.org/10.1038/ncomms8592, 2015.

Rouxel, O., Shanks, W. C., Bach, W., and Edwards, K. J.: Integrated Fe- and S-isotope study of seafloor hydrothermal vents at East Pacific Rise 9–10° N, Chemical Geology, 252, 214–227, https://doi.org/10.1016/j.chemgeo.2008.03.009, 2008.

Rudnick, R. L. and Gao, S.: 4.1 – Composition of the Continental Crust, in: Treatise on Geochemistry (Second Edition), edited by: Holland, H. D. and Turekian, K. K., Elsevier, Oxford, 1–51, https://doi.org/10.1016/B978-0-08-095975-7.00301-6, 2014.

Ryan, J. P., Ueki, I., Chao, Y., Zhang, H., Polito, P. S., and Chavez, F. P.: Western Pacific modulation of large phytoplankton blooms in the central and eastern equatorial Pacific, Journal of Geophysical Research: Biogeosciences, 111, https://doi.org/10.1029/2005JG000084, 2006.

Sarthou, G., Bucciarelli, E., Quéroué, F., Lacan, F., Planquette, H., Pham, V. Q., Grand, M., Pradoux, C., Rodier, M., Bonnet, S., Eldin, G., Cravatte, S., Jeandel, C., and Ganachaud, A.: Dissolved iron distribution and budget in the Solomon Sea, Marine Chemistry, 273, 104567, https://doi.org/10.1016/j.marchem.2025.104567, 2025.

Schlitzer, R.: Ocean Data View, https://odv.awi.de (last access: 30 December 2025), 2025.

Severmann, S., Johnson, C. M., Beard, B. L., German, C. R., Edmonds, H. N., Chiba, H., and Green, D. R. H.: The effect of plume processes on the Fe isotope composition of hydrothermally derived Fe in the deep ocean as inferred from the Rainbow vent site, Mid-Atlantic Ridge, 36°14′ N, Earth Planet Sc. Lett., 225, 63–76, https://doi.org/10.1016/j.epsl.2004.06.001, 2004.

Severmann, S., Johnson, C. M., Beard, B. L., and McManus, J.: The effect of early diagenesis on the Fe isotope compositions of porewaters and authigenic minerals in continental margin sediments, Geochim. Cosmochim. Ac., 70, 2006–2022, https://doi.org/10.1016/j.gca.2006.01.007, 2006.

Sharma, M., Polizzotto, M., and Anbar, A. D.: Iron isotopes in hot springs along the Juan de Fuca Ridge, Earth Planet Sc. Lett., 194, 39–51, https://doi.org/10.1016/S0012-821X(01)00538-6, 2001.

Sieber, M., Conway, T. M., de Souza, G. F., Hassler, C. S., Ellwood, M. J., and Vance, D.: Isotopic fingerprinting of biogeochemical processes and iron sources in the iron-limited surface Southern Ocean, Earth Planet Sc. Lett., 567, 116967, https://doi.org/10.1016/j.epsl.2021.116967, 2021.

Sieber, M., Lanning, N. T., Steffen, J. M., Bian, X., Yang, S.-C., Lee, J. M., Weiss, G., Hunt, H. R., Charette, M. A., Moore, W. S., Hautala, S. L., Hatta, M., Lam, P. J., John, S. G., Fitzsimmons, J. N., and Conway, T. M.: Long Distance Transport of Subsurface Sediment-Derived Iron From Asian to Alaskan Margins in the North Pacific Ocean, Geophys. Res. Lett., 51, e2024GL110836, https://doi.org/10.1029/2024GL110836, 2024.

Slemons, L., Gorgues, T., Aumont, O., Menkes, C., and Murray, J. W.: Biogeochemical impact of a model western iron source in the Pacific Equatorial Undercurrent, Deep Sea Research Part I: Oceanographic Research Papers, 56, 2115–2128, https://doi.org/10.1016/j.dsr.2009.08.005, 2009.

Slemons, L., Murray, J. W., Resing, J., Paul, B., and Dutrieux, P.: Western Pacific coastal sources of iron, manganese, and aluminum to the Equatorial Undercurrent, Global Biogeochem. Cy., 24, https://doi.org/10.1029/2009GB003693, 2010.

Slemons, L., Paul, B., Resing, J., and Murray, J. W.: Particulate iron, aluminum, and manganese in the Pacific equatorial undercurrent and low latitude western boundary current sources, Mar. Chem., 142–144, 54–67, https://doi.org/10.1016/j.marchem.2012.08.003, 2012.

Sofen, L. E., Antipova, O. A., Buck, K. N., Caprara, S., Chacho, L., Johnson, R. J., Kim, G., Morton, P., Ohnemus, D. C., Rauschenberg, S., Sedwick, P. N., Tagliabue, A., and Twining, B. S.: Authigenic Iron Is a Significant Component of Oceanic Labile Particulate Iron Inventories, Global Biogeochemical Cycles, 37, e2023GB007837, https://doi.org/10.1029/2023GB007837, 2023.

Sokolov, S. and Rintoul, S.: Circulation and water masses of the southwest Pacific: WOCE Section P11, Papua New Guinea to Tasmania, J. Mar. Res., 58, 2000.

Stramma, L. and England, M. H.: On the water masses and mean circulation of the South Atlantic Ocean, J. Geophys. Res.-Oceans, 104, 20863–20883, https://doi.org/10.1029/1999JC900139, 1999.

Sutak, R., Camadro, J.-M., and Lesuisse, E.: Iron Uptake Mechanisms in Marine Phytoplankton, Front. Microbiol., 11, https://doi.org/10.3389/fmicb.2020.566691, 2020.

Swanner, E. D., Bayer, T., Wu, W., Hao, L., Obst, M., Sundman, A., Byrne, J. M., Michel, F. M., Kleinhanns, I. C., Kappler, A., and Schoenberg, R.: Iron Isotope Fractionation during Fe(II) Oxidation Mediated by the Oxygen-Producing Marine Cyanobacterium Synechococcus PCC 7002, Environ. Sci. Technol., 51, 4897–4906, https://doi.org/10.1021/acs.est.6b05833, 2017.

Tagliabue, A., Buck, K. N., Sofen, L. E., Twining, B. S., Aumont, O., Boyd, P. W., Caprara, S., Homoky, W. B., Johnson, R., König, D., Ohnemus, D. C., Sohst, B., and Sedwick, P.: Authigenic mineral phases as a driver of the upper-ocean iron cycle, Nature, 620, 104–109, https://doi.org/10.1038/s41586-023-06210-5, 2023.

Talley, L. D.: Some aspects of ocean heat transport by the shallow, intermediate and deep overturning circulations, Geoph. Monog. Series, 112, 1–22, https://doi.org/10.1029/GM112p0001, 1999.

Talley, L. D.: Freshwater transport estimates and the global overturning circulation: Shallow, deep and throughflow components, Prog. Oceanogr., 78, 257–303, https://doi.org/10.1016/j.pocean.2008.05.001, 2008.

Talley, L. D., Pickard, G. L., Emery, W. J., and Swift, J. H.: Descriptive Physical Oceanography: An Introduction, Academic Press, 555 pp., ISBN 978-0-7506-4552-2, 2011.

Tian, H.-A., van Manen, M., Bunnell, Z. B., Jung, J., Lee, S. H., Kim, T.-W., Reichart, G.-J., Conway, T. M., and Middag,

R.: Biogeochemistry of iron in coastal Antarctica: isotopic insights for external sources and biological uptake in the Amundsen Sea polynyas, Geochim. Cosmochim. Ac., 363, 51–67, https://doi.org/10.1016/j.gca.2023.10.029, 2023.

Tiangang, W., Kumul, C., Yuhao, Z., Mosusu, N., Bimin, Z., Pei, N., and De Vivo, B.: National-scale Geochemical Baseline of 69 elements in Papua New Guinea stream sediments, J. Geochem. Explor., 256, 107355, https://doi.org/10.1016/j.gexplo.2023.107355, 2024.

Tomczak, M. and Godfrey, J. S.: Regional Oceanography: An Introduction, Daya Publishing House, 410 pp., ISBN 978-81-7035-306-5, 2003.

Tomczak, M. and Hao, D.: Water masses in the thermocline of the coral sea, Deep-Sea Res., 36, 1503–1514, https://doi.org/10.1016/0198-0149(89)90054-X, 1989.

Tsuchiya, M.: The Origin of the Pacific Equatorial 13 °C Water, J. Phys. Oceanogr., 11, 794–812, https://doi.org/10.1175/1520-0485(1981)011<0794:TOOTPE>2.0.CO;2, 1981.

Tsuchiya, M.: Flow path of the Antarctic Intermediate Water in the western equatorial South Pacific Ocean, Deep-Sea Res., 38, S273–S279, https://doi.org/10.1016/S0198-0149(12)80013-6, 1991.

Tsuchiya, M. and Talley, L.: Water-property distributions along an eastern Pacific hydrographic section at 135W, J. Mar. Res., 54, https://elischolar.library.yale.edu/journal_of_marine_research/2191 (last access: 4 March 2024), 1996.

Tsuchiya, M., Lukas, R., Fine, R. A., Firing, E., and Lindstrom, E.: Source waters of the Pacific Equatorial Undercurrent, Prog. Oceanogr., 23, 101–147, https://doi.org/10.1016/0079-6611(89)90012-8, 1989.

Waeles, M., Baker, A. R., Jickells, T., and Hoogewerff, J.: Global dust teleconnections: aerosol iron solubility and stable isotope composition, Environ. Chem., 4, 233, https://doi.org/10.1071/EN07013, 2007.

Wilson, E. L., Harpp, K. S., Schwartz, D. M., and Van Kirk, R.: The Geochemical Evolution of Santa Cruz Island, Galápagos Archipelago, Front. Earth Sci., 10, https://doi.org/10.3389/feart.2022.845544, 2022.

Winckler, G., Anderson, R. F., Jaccard, S. L., and Marcantonio, F.: Ocean dynamics, not dust, have controlled equatorial Pacific productivity over the past 500,000 years, P. Natl. Acad. Sci. USA, 113, 6119–6124, https://doi.org/10.1073/pnas.1600616113, 2016.

Wyrtki, K.: The Subsurface Water Masses in the Western South Pacific Ocean, Mar. Freshwater Res., 13, 18–47, https://doi.org/10.1071/mf9620018, 1962.

Yeghicheyan, D., Bossy, C., Bouhnik Le Coz, M., Douchet, C., Granier, G., Heimburger, A., Lacan, F., Lanzanova, A., Rousseau, T. C. C., Seidel, J.-L., Tharaud, M., Candaudap, F., Chmeleff, J., Cloquet, C., Delpoux, S., Labatut, M., Losno, R., Pradoux, C., Sivry, Y., and Sonke, J. E.: A Compilation of Silicon, Rare Earth Element and Twenty-One other Trace Element Concentrations in the Natural River Water Reference Material SLRS-5 (NRC-CNRC), Geostand. Geoanal. Res., 37, 449–467, https://doi.org/10.1111/j.1751-908X.2013.00232.x, 2013.

Yeghicheyan, D., Aubert, D., Bouhnik-Le Coz, M., Chmeleff, J., Delpoux, S., Djouraev, I., Granier, G., Lacan, F., Piro, J.-L., Rousseau, T., Cloquet, C., Marquet, A., Menniti, C., Pradoux, C., Freydier, R., Vieira da Silva-Filho, E., and Suchorski, K.: A New Interlaboratory Characterisation of Silicon, Rare Earth Elements and Twenty-Two Other Trace Element Concentrations in the Natural River Water Certified Reference Material SLRS-6 (NRC-CNRC), Geostand. Geoanal. Res., 43, 475–496, https://doi.org/10.1111/ggr.12268, 2019.

Yuan, X. and Talley, L. D.: Shallow Salinity Minima in the North Pacific, J. Phys. Oceanogr., 22, 1302–1316, https://doi.org/10.1175/1520-0485(1992)022<1302:SSMITN>2.0.CO;2, 1992.

Zheng, L. and Sohrin, Y.: Major lithogenic contributions to the distribution and budget of iron in the North Pacific Ocean, Sci. Rep., 9, 11652, https://doi.org/10.1038/s41598-019-48035-1, 2019.